The Astrophysical Journal, 746:136 (23pp), 2012 February 20 doi:10.1088/0004-637X/746/2/136

THE *HST*/ACS COMA CLUSTER SURVEY. VIII. BARRED DISK GALAXIES IN THE CORE OF THE COMA CLUSTER*

Irina Marinova[1], Shardha Jogee[1], Tim Weinzirl[1], Peter Erwin[2,3], Neil Trentham[4], Henry C. Ferguson[5], Derek Hammer[6], Mark den Brok[7], Alister W. Graham[8], David Carter[9], Marc Balcells[10], Paul Goudfrooij[5], Rafael Guzmán[11], Carlos Hoyos[11], Bahram Mobasher[12], Mustapha Mouhcine[9], Reynier F. Peletier[7], Eric W. Peng[13,14], and Gijs V. Kleijn[7]

[1] Department of Astronomy, University of Texas at Austin, Austin, TX, USA; marinova@astro.as.utexas.edu, sj@astro.as.utexas.edu
[2] Max-Planck-Insitut für extraterrestrische Physik, Giessenbachstrasse, 85748 Garching, Germany
[3] Universitäts-Sternwarte München, Scheinerstrasse 1, 81679 München, Germany
[4] Institute of Astronomy, Madingley Road, Cambridge, CB3 0HA, UK
[5] Space Telescope Science Institute, 3700 San Martin Drive, Baltimore, MD 21218, USA
[6] Department of Physics and Astronomy, Johns Hopkins, Baltimore, MD 21218, USA
[7] Kapteyn Astronomical Institute, University of Groningen, Groningen, The Netherlands
[8] Centre for Astrophysics and Supercomputing, Swinburne University, Hawthorn, Australia
[9] Astrophysics Research Institute, Liverpool John Moores University, Birkenhead, UK
[10] Instituto de Astrofísica de Canarias, 38200 La Laguna, Tenerife, Spain
[11] Department of Astronomy, University of Florida, Gainesville, FL 32611, USA
[12] Department of Physics and Astronomy, University of California, Riverside, CA 92521, USA
[13] Department of Astronomy, Peking University, Beijing 100871, China
[14] Kavli Institute for Astronomy and Astrophysics, Peking University, Beijing 100871, China
Received 2011 June 24; accepted 2011 December 25; published 2012 February 1

ABSTRACT

We use high-resolution (∼0.″1) F814W Advanced Camera for Surveys (ACS) images from the *Hubble Space Telescope* ACS Treasury survey of the Coma cluster at $z \sim 0.02$ to study bars in massive disk galaxies (S0s), as well as low-mass dwarf galaxies in the core of the Coma cluster, the densest environment in the nearby universe. Our study helps to constrain the evolution of bars and disks in dense environments and provides a comparison point for studies in lower density environments and at higher redshifts. Our results are: (1) we characterize the fraction and properties of bars in a sample of 32 bright ($M_V \lesssim -18$, $M_* > 10^{9.5}\ M_\odot$) S0 galaxies, which dominate the population of massive disk galaxies in the Coma core. We find that the measurement of a bar fraction among S0 galaxies must be handled with special care due to the difficulty in separating unbarred S0s from ellipticals, and the potential dilution of the bar signature by light from a relatively large, bright bulge. The results depend sensitively on the method used: the bar fraction for bright S0s in the Coma core is 50% ± 11%, 65% ± 11%, and 60% ± 11% based on three methods of bar detection, namely, strict ellipse fit criteria, relaxed ellipse fit criteria, and visual classification. (2) We compare the S0 bar fraction across different environments (the Coma core, A901/902, and Virgo) adopting the critical step of using matched samples and matched methods in order to ensure robust comparisons. We find that the bar fraction among bright S0 galaxies does not show a statistically significant variation (within the error bars of ±11%) across environments which span two orders of magnitude in galaxy number density ($n \sim$ 300–10,000 galaxies Mpc^{-3}) and include rich and poor clusters, such as the core of Coma, the A901/902 cluster, and Virgo. We speculate that the bar fraction among S0s is not significantly enhanced in rich clusters compared to low-density environments for two reasons. First, S0s in rich clusters are less prone to bar instabilities as they are dynamically heated by harassment and are gas poor as a result of ram pressure stripping and accelerated star formation. Second, high-speed encounters in rich clusters may be less effective than slow, strong encounters in inducing bars. (3) We also take advantage of the high resolution of the ACS (∼50 pc) to analyze a sample of 333 faint ($M_V > -18$) dwarf galaxies in the Coma core. Using visual inspection of unsharp-masked images, we find only 13 galaxies with bar and/or spiral structure. An additional eight galaxies show evidence for an inclined disk. The paucity of disk structures in Coma dwarfs suggests that either disks are not common in these galaxies or that any disks present are too hot to develop instabilities.

Key words: galaxies: evolution – galaxies: fundamental parameters – galaxies: kinematics and dynamics – galaxies: structure

Online-only material: color figures

1. INTRODUCTION

Mounting evidence suggests that at $z \sim 1$, major mergers among massive galaxies are not very frequent (e.g., Bell et al. 2006; Jogee et al. 2009; Robaina et al. 2009; Weinzirl et al. 2009) and have not contributed significantly to the cosmic star formation rate (SFR) density (e.g., Bell et al. 2005; Wolf et al. 2005; Jogee et al. 2009; Robaina et al. 2009) or to the building of bulges in massive spirals (Weinzirl et al. 2009; Kormendy & Fisher 2008; Laurikainen et al. 2007) since $z < 1$. Other processes, such as minor mergers (Jogee et al. 2009; Weinzirl et al. 2009) or internal secular processes (Laurikainen et al. 2007; Kormendy & Fisher 2008) are increasingly invoked.

* Based on observations with the NASA/ESA *Hubble Space Telescope* obtained at the Space Telescope Science Institute, which is operated by the Association of Universities for Research in Astronomy, Inc., under NASA contract NAS 5-26555. These observations are associated with program GO10861.

The most efficient internal driver of evolution in disk galaxies is stellar bars. They effectively redistribute angular momentum in the disk and dark matter (DM) halo, and drive large gas inflows to the central regions of galaxies. The resulting central dense gas concentrations ignite powerful starbursts (Schwarz 1981; Sakamoto et al. 1999; Jogee 1999; Jogee et al. 2005; Sheth et al. 2005). In this way, bars are thought to build disky central components known as pseudobulges (Hohl 1975; Kormendy 1979, 1993; Combes & Sanders 1981; Combes et al. 1990; Jogee 1999, Jogee et al. 2005).

We describe below some of the recent progress made in exploring the bar fraction (defined as the fraction of disk galaxies hosting a large-scale bar) in terms of methodology, dependence on Hubble type, redshift, and environment. For a long time, statistics on the optical bar fraction in the local universe came from visual classification of the galaxies in the Third Reference Catalog of Bright Galaxies (RC3; de Vaucouleurs et al. 1991). In the RC3, over all disk galaxies (S0–Im), the visual optical bar fraction is ∼30% for strong bars (SB) and ∼30% for weak bars (SAB) giving ∼60% overall. The RC3 optical bar fraction suffers from two limitations: first, it denotes the optical bar fraction averaged over a broad range of Hubble types and second, it is based on visual classification to identify and characterize bars, thus giving no quantitative measurements of their properties (such as size, shape, strength). In fact, the former limitation has persisted in many recent studies which focus on the average bar fraction over disks of all Hubble types (Eskridge et al. 2000; Knapen et al. 2000; Hunt & Malkan 1999; Mulchaey & Regan 1997; Laine et al. 2002; Laurikainen et al. 2004; Block et al. 2004; although see Odewahn 1996).

Recent studies have made important headway on both fronts. First, quantitative methods such as ellipse fitting (e.g., Wozniak et al. 1995, Friedli et al. 1996; Regan & Elmegreen 1997; Mulchaey & Regan 1997; Jogee 1999, Jogee et al. 2002a, 2002b, 2004; Knapen et al. 2000; Laine et al. 2002; Sheth et al. 2003, 2008; Elmegreen et al. 2004; Menéndez-Delmestre et al. 2007; Marinova & Jogee 2007, hereafter MJ07; Aguerri et al. 2009) and bulge-bar–disk decomposition (e.g., Laurikainen et al. 2005; Reese et al. 2007, Weinzirl et al. 2009, Gadotti 2011) are being used to reduce the level of subjectivity. Second, evidence is mounting that the bar fraction varies across galaxies of different Hubble types (Barazza et al. 2008, hereafter BJM08; Aguerri et al. 2009; Marinova et al. 2009, hereafter M09) and depends non-monotonically on the host galaxy properties, such as bulge-to-total ratio (B/T), luminosity, stellar mass, and color, at a range of redshifts and environments (M09; Barazza et al. 2009; Weinzirl et al. 2009; Laurikainen et al. 2009; Nair & Abraham 2010a; Cameron et al. 2010; Gadotti 2011).

Most of the results described above have focused on field galaxies at low redshifts, while much less is known about barred disks at higher redshifts (Abraham et al. 1999; Sheth et al. 2003; Jogee et al. 2004; Sheth et al. 2008; Cameron et al. 2010) and in dense environments. Dense environments such as clusters can be an important laboratory for studying the co-evolution of bars and their host disks, as there are many physical processes, which are unique to such environments and impact disks and bars. For example, we can study how the cumulative effect of frequent weak galaxy encounters ("harassment"; Moore et al. 1996), the effect of the intracluster medium (ICM) on galaxies (Gunn & Gott 1972; Larson et al. 1980; Quilis et al. 2000), and the influence of the cluster potential as a whole (e.g., Byrd & Valtonen 1990; Gnedin 2003) affect the properties of bars and disks. Theoretical studies exploring these processes give conflicting predictions. For example, although the numerous tidal encounters in a dense cluster core can induce bars in unbarred disks in the case of a prograde encounter, they can also have little or no effect in terms of inducing a bar (or affecting the strength of an already existing bar) in the case of retrograde encounters (Gerin et al. 1990; Romano-Díaz et al. 2008; Aguerri & González-García 2009). Determining the fraction and properties of barred galaxies in such extreme environments and comparing them to those of galaxies in environments of varying densities can give clues to the outstanding problems in understanding the formation and growth of bar instabilities in disks, and therefore to understanding disk evolution. In addition, identifying barred disks in cluster environments can provide a lower limit to the fraction of disk systems in clusters (e.g., M09; Méndez-Abreu et al. 2010).

Quantitative results addressing this issue are only starting to emerge. Several recent studies of non-dwarf galaxies at a range of redshifts from $0.01 < z < 0.4$ (Barazza et al. 2009; Aguerri et al. 2009; M09) find that the optical bar fraction shows at most a modest variation (±10%) between field and intermediate-density environments (e.g., moderately rich clusters). But what happens at really high densities (i.e., dense cluster cores)? Some studies (Thompson 1981; Andersen 1996; Barazza et al. 2009) have suggested that, within a galaxy cluster, the bar fraction may be higher in the dense core regions than the outskirts. However, this has remained an open question for cluster cores due to issues such as limited number statistics, projection effects, poor quality or inhomogeneous data, and uncertainties in cluster membership. We make progress in two ways with this study. First, we are able to establish cluster membership for all galaxies in our bright S0 sample (see Section 3) using spectroscopic redshifts. Although we are still limited by line-of-sight projection effects from within the Coma cluster itself, the number density of galaxies in the core of Coma is a factor of 10–100 times higher than at larger cluster radii, so we expect the impact of such line-of-sight contamination to be low. Second, the high-resolution *Hubble Space Telescope*(*HST*) Advanced Camera for Surveys (ACS) data are vital in identifying bars in S0s, especially in the types of cases we discuss in Section 3.2.2, namely, where a relatively large bulge in combination with a relatively short bar and projection effects combine to make bar detection difficult in low-resolution ground-based images.

In this paper, we provide baseline results for the densest environment in the local universe: the central regions of Coma. We conduct two explorations using two different samples. In the first part of this paper (Section 3), we focus on the sample of bright ($M_V \lesssim -18$) non-dwarf S0 galaxies, which comprise 94% of our sample of bright disk galaxies in the Coma core. We characterize their disk and bar properties and present results on the optical bar fraction for bright S0 galaxies from ellipse fitting and visual classification. We compare with the results of other studies of S0 galaxies in Coma and less dense clusters (A901/902 and Virgo).

In the second part of this paper (Section 4), we take advantage of the exquisite 50 pc resolution of the ACS images to search for bars and other disk features (spiral arms, inclined disks) in the faint, dwarf ($M_V > -18$) galaxies of the Coma cluster core. The prevalence or paucity of bar structures in early-type dwarf galaxies cannot only provide clues on the evolutionary history of these dwarf systems, but also has implications for the conditions necessary for bar formation and growth in galaxies. Are bar/spiral arm instabilities commonplace for dwarf galaxies? Some early-type dwarfs in clusters are believed to have

originated from late-type spirals or dwarf irregulars (e.g., Lin & Faber 1983; Kormendy 1985) that have been stripped of their gas by external processes. This is especially true in a cluster setting where environmental processes like ram-pressure stripping and harassment are commonplace. If the progenitor galaxy hosted a stellar bar or spiral arms, these stellar features can persist even after the galaxy's gas has been processed by the cluster environment. In fact, a number of early-type dwarf galaxies in Virgo have been observed to host stellar disk features such as a lens, a bar, or spiral arms (e.g., Sandage & Binggeli 1984; Binggeli & Cameron 1991; Jerjen et al. 2000; Barazza et al. 2002; Lisker et al. 2006, 2007; Lisker & Fuchs 2009) thus supporting the above scenario. Graham et al. (2003) discovered the first two early-type dwarf galaxies with spiral-like structure in the Coma cluster using unsharp masking, concluding that such galaxies may provide the "missing link" in the evolution of faint spiral galaxies into dwarf spheroidals due to cluster processes.

The layout of this paper is as follows: in Section 2, we describe our data set and sample selection. Section 3 deals with our bright ($M_V \lesssim -18$) Coma core sample. In this section we outline our methods for identifying bright S0 galaxies (Section 3.1), our methods for identifying bars in these galaxies (Sections 3.2 and 3.3), our results for S0 galaxies in the Coma core (Sections 3.4–3.7) and the implications of these results for bar and disk formation and evolution in dense environments (Section 3.8). In Section 4, we present our investigation of the faint, dwarf galaxies in our Coma core sample. We describe our methods for finding disk features (bar, spiral arms, inclined disk) in these galaxies (Section 4.2), as well as our results and discussion for dwarf galaxies in Section 4.3. We summarize all of our results in Section 5.

2. DATA AND SELECTION OF A CLUSTER SAMPLE

Our data come from the *HST* ACS Treasury survey of the Coma cluster at $z \sim 0.023$ (Carter et al. 2008). Originally designed to cover a large area of the core and infall region of Coma, the survey remains only ∼28% complete because of the failure of ACS in 2007. Nevertheless, the available data span 274 arcmin^2, where approximately 75% of the data are within 0.5 Mpc of the cluster center. The data cover approximately 70% of the core region of Coma (assuming $R_{\rm core} \sim 0.2$ Mpc) and are therefore representative of the core and the immediate surroundings, namely, the region where the galaxy number density is ∼10,000 galaxies Mpc^{-3} before it drops sharply as a function of distance from the cluster center (The & White 1986). This data set contains thousands of sources down to a limiting magnitude of $I = 26.8$ mag in F814W (AB mag). The ACS point-spread function (PSF) is ∼0.″1, which corresponds to ∼50 pc at the distance of the Coma cluster, assuming a distance of $D = 100$ Mpc.[15] *SExtractor* source catalogs are available as a part of the Coma survey data releases. The second data release (DR2) is described in detail in Hammer et al. (2010). Throughout the paper, $M_{\rm I(814)}$ as well as Sloan Digital Sky Survey (SDSS) g and r magnitudes are given in the AB system, while B and V magnitudes are in the Vega system.

We first use the eyeball catalog of N. Trentham et al. (2012, in preparation) to select cluster members. In this catalog, galaxies are visually assigned a cluster membership class from 0 to 4. Galaxies with membership class 0 are spectroscopically confirmed members, while galaxies with class 4 are visually deemed to be likely background objects. The intermediate membership classes from 1 (very probable cluster member) to 3 (plausible cluster member) are assigned based on a visual estimation taking into account both surface brightness and morphology (N. Trentham et al. 2012, in preparation). We select objects with apparent magnitude $m_{\rm I(814)} \leqslant 24$ (AB mag) and membership class 0–3, resulting in a sample of 469 cluster galaxies. For these galaxies, 41% are spectroscopically confirmed members (class 0), while 7%, 27%, and 25% have membership classes 1–3, respectively.

We derive B and V magnitudes (in Vega mag) for the Coma galaxies using SDSS g and r (in AB mag). For the bright sample, we use the B, V, g, and r magnitudes (instead of the ACS F814W) for ease of comparison to other studies. In addition, Hammer et al. (2010) found that for bright galaxies ($M_{\rm I(814)} \leqslant 17$ AB mag) in the Coma survey, it is more reliable to use the SDSS rather than ACS magnitudes, as the latter may be unreliable for some galaxies with large, diffuse stellar halos. We use the following transformations from Jester et al. (2005) to convert the SDSS g and r (AB) to B and V (Vega)[16]:

$$B = g + 0.39 \times (g - r) + 0.21 \quad (1)$$

$$V = g - 0.59 \times (g - r) - 0.01. \quad (2)$$

We calculate absolute magnitudes assuming a distance modulus of 35.0 (Carter et al. 2008).

In this paper, we explore the optical bar fraction in two regimes: bright, non-dwarf S0 disks (Section 3) and faint (dwarf) galaxies (Section 4). To separate these two regimes, we apply a magnitude cut of $M_{\rm I(814)} \leqslant -18.5$, roughly equivalent to $M_V \lesssim -18$ or $M_B \lesssim -17$ for our sample. We choose a cut at $M_V \sim -18$ because it tends to separate well the regimes where normal and dwarf galaxies dominate on the luminosity functions of clusters (Binggeli et al. 1988; Trentham 1998; Trentham & Hodgkin 2002; Mobasher et al. 2003). Luminosity cuts at magnitudes $M_V \sim -18$ are often used to separate dwarf and non-dwarf galaxies in the literature (Matković & Guzmán 2005; Aguerri et al. 2005; van Zee 2001; Barazza et al. 2006). This cut gives 52 galaxies brighter than and 417 galaxies fainter than $M_V = -18$. From the 52 bright galaxies, we discard four galaxies (two are a close/merging pair and two galaxies are partially off the edge of a tile) bringing our initial bright sample to 48 galaxies. We discuss the methods for selecting S0 galaxies from this bright sample in Section 3.1.

In Figure 1(a), we show the absolute magnitude $M_{\rm I(814)}$ distribution for the non-dwarf (bright) and dwarf Coma core samples. Figure 1(b) shows the peak surface brightness μ_0 (from the *SExtractor* source catalogs in DR2) versus absolute magnitude $M_{\rm I(814)}$ distribution of the bright, non-dwarf and dwarf galaxies.

3. BARS IN BRIGHT S0 GALAXIES IN THE CENTRAL REGION OF THE COMA CLUSTER

3.1. Identifying Bright S0 Galaxies

Due to the fact that bars are inherently a disk phenomenon, the bar fraction is traditionally defined as

$$f_{\rm bar} = \frac{N_{\rm bar}}{N_{\rm bar} + N_{\rm unbar}}, \quad (3)$$

[15] We assume in this paper a flat cosmology with $\Omega_M = 1 - \Omega_\Lambda = 0.3$ and $H_0 = 70$ km s^{-1} Mpc^{-1}.

[16] The transformation equation tables can be found at http://www.sdss.org/dr7/algorithms/sdssUBVRITransform.html.

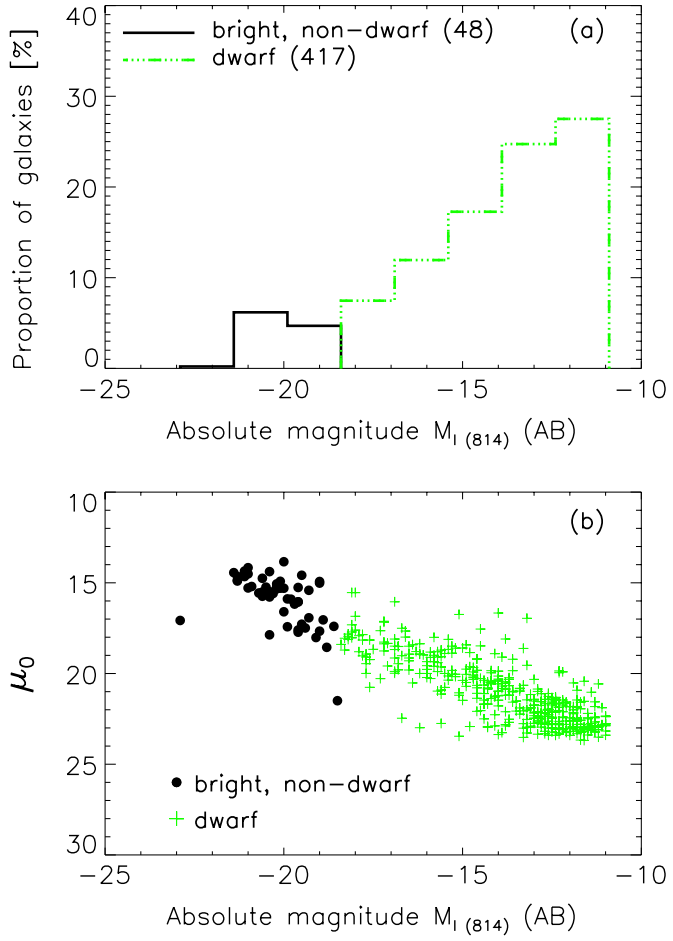

Figure 1. (a) Absolute magnitude ($M_{I(814)}$) distribution of the bright, non-dwarf (black solid line; $M_V \lesssim -18$) and dwarf (green dash-dot line; $M_V > -18$) galaxies in our Coma core cluster member sample (Section 2). Most galaxies are dwarfs with $M_V > -18$. (b) Central surface brightness μ_0 (from the *SExtractor* source catalogs in DR2) vs. absolute magnitude $M_{I(814)}$ for the bright, non-dwarf (black circles) and dwarf (green plus) cluster core samples.

(A color version of this figure is available in the online journal.)

where N_{bar} and N_{unbar} represent the number of barred and unbarred disk galaxies, respectively. Therefore, from the bright sample of 48 galaxies, we need a sample of disk galaxies (e.g., S0–Im) for analysis. As discussed in Section 1, recent work has shown that a bar fraction averaged over a wide range in Hubble types gives only limited information. The bar fraction is a strong function of galaxy properties, such as B/T, luminosity, stellar mass, and color. Because our sample is too small to split into fine bins by morphological type, and because most (94%) of bright disk galaxies in our Coma core sample are S0s (see below), *our analysis of bright galaxies in this paper focuses on S0s only*. The goal of our study is to provide the bar fraction for the densest low-redshift ($z \sim 0.02$) environment and to serve as a comparison point for studies of barred S0 galaxies in field and intermediate-density environments at different redshifts.

Starting with the bright sample of 48 galaxies, we use visual classification to separate the galaxies into ellipticals, S0s, visually ambiguous E/S0, and spirals. We note that our visually identified class of "S0" galaxies includes all Hubble type S0 sub-types from S0$^-$ to S0/a (numerical T-types -3 to 0). It is fairly easy to separate S0s and ellipticals visually when the S0s host bars. However, unbarred S0s are harder to separate from ellipticals since an unbarred S0 hosts a disk, which is effectively featureless and devoid of tell-tale disk signatures, such as a bar or spiral arms. We find a group of 10 bright galaxies that are *visually* ambiguous E/S0s. For each of these 10 galaxies, we perform multiple component structural decomposition with the GALFIT code (Peng et al. 2002) by fitting the two-dimensional (2D) light distribution taking into account the PSF, following the procedure described in Weinzirl et al. (2009). In brief, we fitted each galaxy with three models: a single-component Sérsic model, a two-component ("bulge"+disk) model, and a three component ("bulge"+disk+bar) model. The disk is represented by an exponential (Sérsic $n = 1$) model, while the "bulge" is a Sérsic model with a free-floating Sérsic index n. The bar is typically associated with a Sérsic model of low n. If needed, a point source component was added to represent the point sources, which are common in the center of these galaxies. For each model, GALFIT finds the optimum solution using the Levenberg–Marquardt algorithm. The goodness of fit is determined iteratively by calculating χ^2. GALFIT continues to adjust the model parameters until the gradient $\delta\chi^2/\chi^2$ is very small (e.g., 10^{-4}) for 10 continuous iterations. Out of the three models (Sérsic, "bulge"+disk, "bulge"+disk+bar), the best one was selected by considering a number of factors, including the χ^2 values, the strength and spatial distribution of the residuals, and the physical viability of output parameters (e.g., effective radii of the Sérsic and bulge component; scale length, axial ratio, and position angle (PA) of the disk). These factors were used to decide whether the galaxy is likely an elliptical or an S0. Examples of the data, model, and residuals for three representative galaxies classified as E, S0/a, and E/S0 after decomposition are shown in Figure 2.

Out of the 10 *visually* ambiguous E/S0 galaxies, we find from multi-component decompositions that one is an elliptical, eight are S0 or S0/a, and one is still ambiguous E/S0. The ambiguous galaxy may be a disk galaxy with complex structure or an elliptical with an inner debris disk. In Section 3.4, we use this galaxy to estimate the uncertainty in the optical bar fraction by calculating f_{bar} (see Equation (1)) for the two cases where this galaxy is either included or excluded in the number of unbarred disks (N_{unbar}).

The absolute magnitude $M_{I(814)}$ distribution of the bright Coma core sample is shown in Figure 3(a). The final morphological breakdown of our bright sample (13 ellipticals, 1 ambiguous E/S0, 32 S0s, and 2 spirals) is shown in Figure 3(b). It is clear that S0s dominate among the bright disk galaxies in our Coma core sample, which is expected for the central regions of a dense cluster. We find a ratio of E:S0:Sp of 28%:68%:4%. This is at the extreme end of the morphology–density relation found in dense environments by Dressler (1980). Figure 3(c) shows the distribution of stellar mass for the S0 disk sample as well as all bright ($M_V \lesssim -18$) galaxies. Stellar masses are calculated using the relations from Borch et al. (2006)[17] assuming a Kroupa et al. (1993) initial mass function (IMF):

$$\frac{M}{M_\odot} = \upsilon_{lum} \times 10^{-0.628+1.305(B-V)-0.1}, \quad (4)$$

where

$$\upsilon_{lum} = 10^{-0.4(V-4.82)}. \quad (5)$$

[17] The Kroupa IMF offset term is reported as -0.15 in Bell et al. (2003). However this value was calculated assuming unrealistic conditions (E. Bell 2011, private communication). The correct value of -0.1 was recalculated and reported in Borch et al. (2006).

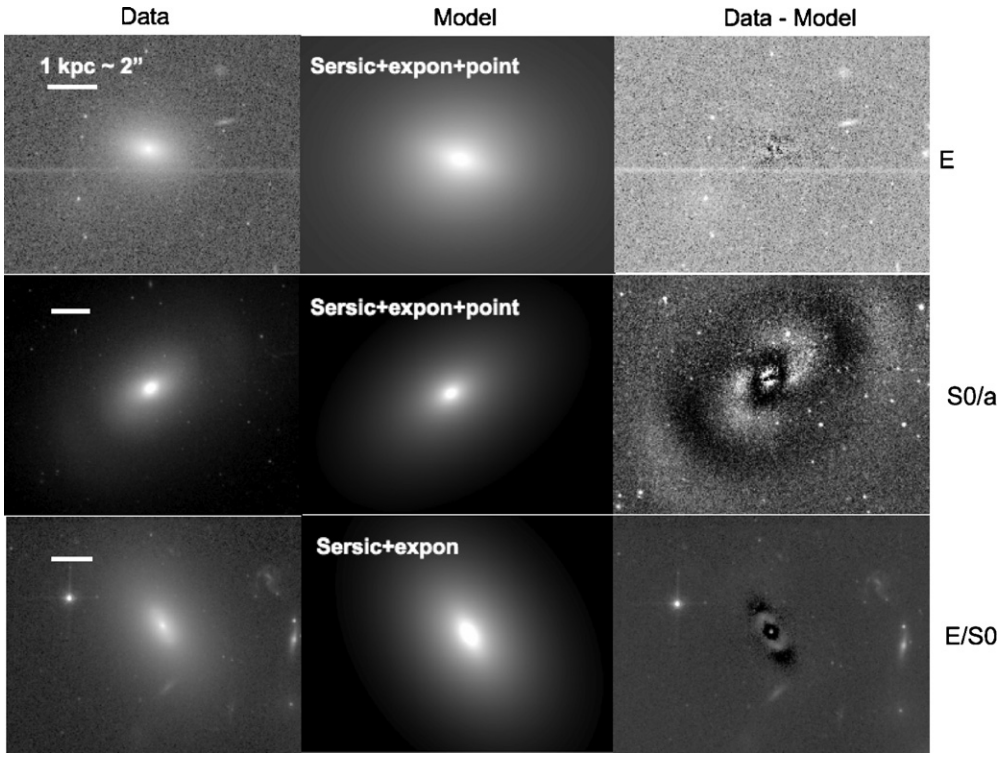

Figure 2. For the 10 visually ambiguous E/S0 galaxies, single and multiple component decompositions were performed with GALFIT on the two-dimensional light distribution to help determine whether they are an elliptical (E) or S0. This figure shows examples of the data (left), GALFIT model (middle), and (data-model) residuals (right) for three of these galaxies, which ended up being classified after decomposition (Section 3.1) as E (top row), S0/a (middle row), and still ambiguous E/S0 (bottom row). For the galaxy (COMAi125930.268p28115.17) in the top row the best-fit model consists of a Sérsic component of half light radius $R_e \sim 1.4$ kpc, within which is embedded a compact disk and a nuclear point source. This galaxy does not make the cut to be an S0 as it lacks a bulge and extended outer disk, and it is not included in the analysis of the bar fraction for S0s. The galaxy in the second row (COMAi125938.323p275913.84) is classified as an S0/a because after fitting a (Sérsic+Exponential) model, corresponding to a bulge and extended outer disk, one can see extended spiral structure in the residuals. Since spiral structures only exist in disks, this confirms the presence of an outer disk. We classify this galaxy as an S0/a rather than an Sa because the spiral structure is revealed in the residuals and is not readily visible on the direct image. The galaxy (COMAi125950.103p275529.47) in the third row is classified as an ambiguous E/S0 because, based on the residuals and other factors (χ^2 and fit parameters), it is still not possible to determine whether this galaxy is more likely to be an elliptical with an inner debris disk or an S0.

Galaxies in our S0 disk sample have stellar masses between $10^{9.5}$ and $10^{11} M_{\odot}$. Figure 3(d) shows a $g-r$ color versus $M_{\rm r}$ magnitude diagram. Almost all ellipticals and most disk galaxies fall on the red sequence. We overplot the relation from Blanton et al. (2005) for the break between the red sequence and blue cloud using the equation (modified with an offset of −0.77 for $h = 0.7$)

$$(g-r) = 0.65\text{–}0.03(M_{\rm r} - 0.77 + 20). \quad (6)$$

We also plot a subsample of the dwarf galaxies ($M_{\rm V} > -18$) for which SDSS data are available (∼30%).

We show examples from our final bright S0 sample of 32 galaxies in Figure 4. We note that all 32 S0s in the bright sample are spectroscopically confirmed cluster members.

3.2. Identification of Bars in S0s via Ellipse Fits

Ellipse fitting is our primary method of detecting bars in the bright S0 sample (e.g., Wozniak et al. 1995, Friedli et al. 1996; Regan et al. 1997; Mulchaey & Regan 1997; Jogee 1999, Jogee et al. 2002a, 2002b, 2004; Knapen et al. 2000; Laine et al. 2002; Sheth et al. 2003, 2008; Elmegreen et al. 2004; Menéndez-Delmestre et al. 2007; MJ07; Aguerri et al. 2009). To detect bars through ellipse fitting we use the standard IRAF task *ELLIPSE* in conjunction with an adaptive wrapper (Jogee et al. 2004), which runs *ELLIPSE* iteratively on each galaxy until the best fit is found or up to a maximum number of times specified by the user. Ellipses are fit to the galaxy isophotes out to a maximum distance ($a_{\rm disk}$) where the brightness of the isophotes reaches the noise level. We note that the value of $a_{\rm disk}$ depends on the depth of the image, as $a_{\rm disk}$ will reach larger values for deeper images. However for the purpose of bar detection, it is only necessary for the radial profile to extend beyond the bar into the more circular region of the disk. We typically set the maximum allowed iterations to 300, however for most galaxies a good fit is achieved in only a few iterations. A good fit is one where an ellipse can be fitted at every isophote out to $a_{\rm disk}$. Residuals characterizing how well each isophote is fitted by its corresponding ellipse are given by the harmonic amplitudes A3, B3, A4, and B4 (e.g., Carter 1978; Jedrzejewski 1987; Carter 1987). For our barred galaxies, we find typical amplitudes of 5%–10%. For a detailed discussion on the advantages and drawbacks of using ellipse fitting to characterize bars we refer the reader to MJ07.

Once the galaxies are fitted, we use an interactive visualization tool to display the overlays of the fit on the galaxy image, as well as the radial profiles of surface brightness, ellipticity (e), and PA Using the radial profiles of ellipticity (e) and PA, we classify the galaxies as "highly inclined," "barred," or "unbarred." We discuss these classes in more detail below.

3.2.1. Detecting and Removing Highly Inclined Galaxies

In studies of bars, it is conventional to exclude highly inclined galaxies as the large inclination precludes accurate structural classification, making it particularly difficult to identify systems

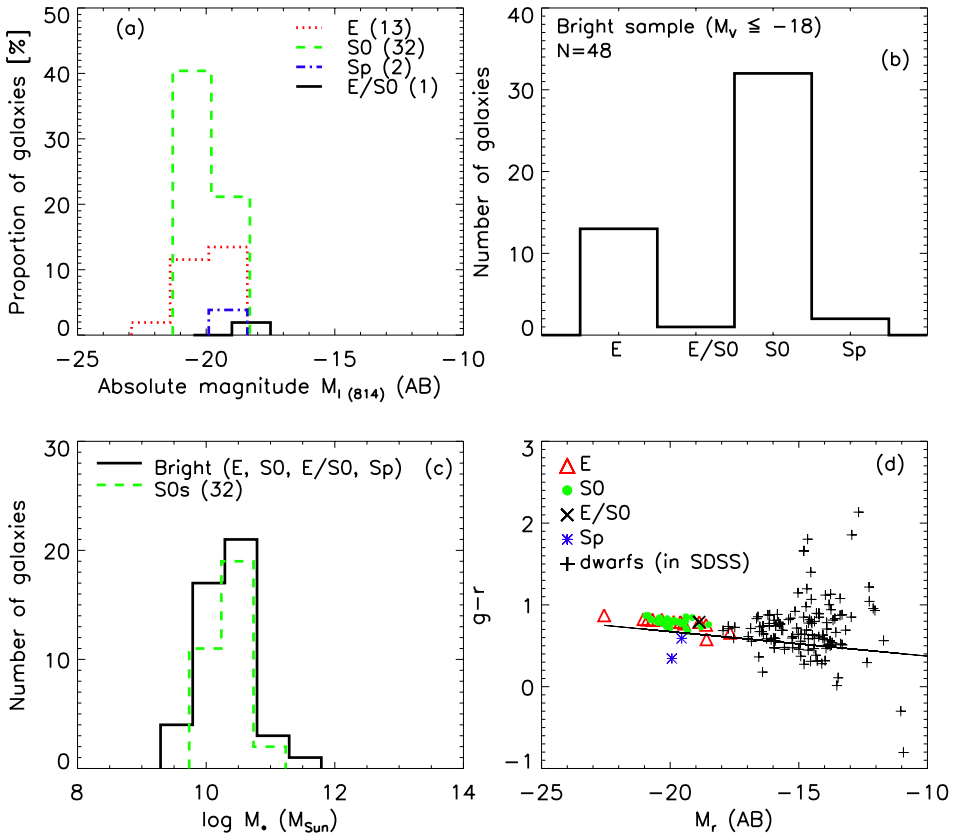

Figure 3. (a) Absolute magnitude distribution of bright ($M_V \leqslant -18$) galaxies in our Coma core sample (Section 3.1). (b) Distribution of morphological types (E, E/S0, S0, Sp) in the bright non-dwarf sample. S0 galaxies (32) comprise 94% of the bright disk galaxies. Morphological types are from visual classification, supplemented with two-dimensional, multi-component decomposition for visually ambiguous cases (Section 3.1). (c) Stellar mass distribution of the bright galaxies in our Coma core sample, with the S0 galaxies shown in green. The S0s have masses between $10^{9.5}$ and 10^{11} $M_\odot$. (d) $g - r$ color–magnitude diagram of the bright cluster sample and a subset (30%) of the dwarf sample with available SDSS magnitudes. We overplot the relation from Blanton et al. (2005) for the break between the red sequence and blue cloud. Most elliptical and S0 galaxies lie on the red sequence.

(A color version of this figure is available in the online journal.)

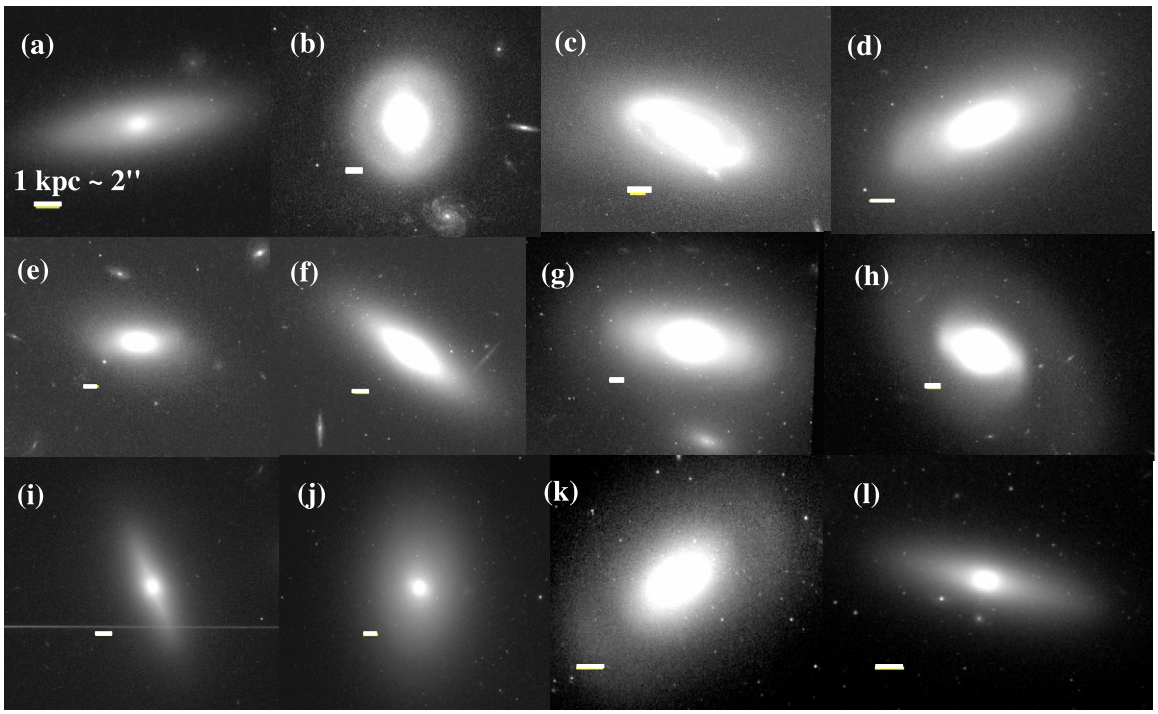

Figure 4. Examples of some S0 galaxies from our bright sample (Section 3.1). The scale bars show 1 kpc. The galaxies shown are: (a) COMAi125704.336p273133.26, (b) COMAi125710.767p272417.44, (c) COMAi125833.136p272151.77, (d) COMAi125832.060p272722.85, (e) COMAi125928.728p28225.90, (f) COMAi125929.404p275100.51, (g) COMAi125929.956p275723.26, (h) COMAi125930.825p275303.42, (i) COMAi125931.455p28247.62, (j) COMAi125932.789p275900.95, (k) COMAi125938.323p275913.84, (l) COMAi125939.657p275713.86.

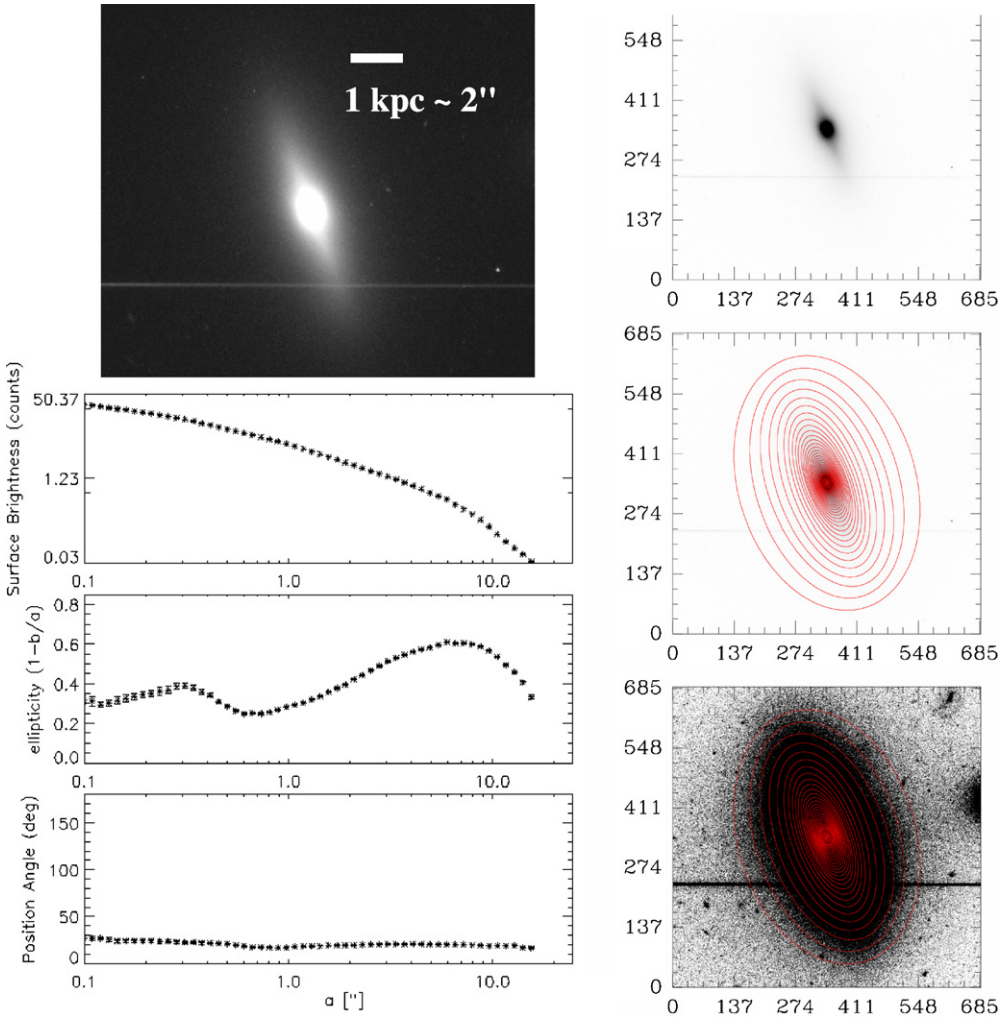

Figure 5. Left: *HST* image and radial profiles of surface brightness, e, and PA of a highly inclined S0 with an outer, diffuse, thickened stellar component (see Section 3.2.1). Right: the ellipse fits are overlaid onto the galaxy image. The top two panels are shown with a stretch that enhances the thin disk and boxy bulge, while the bottom panel shows the outer disk. The thickened, diffuse, outer stellar component causes the outermost isophotes to have $e \sim 0.4$, which is less than the quantitative inclination cut of $e > 0.5$. Therefore, we classify this galaxy as highly inclined using visual classification according to the criteria outlined in Section 3.2.1. (A color version of this figure is available in the online journal.)

as barred or unbarred. We use two ways to identify highly inclined galaxies in the bright S0 sample. The first is via the ellipse fit criteria, where the observed outermost disk isophote (at $a_{\rm disk}$) has $e > 0.5$, corresponding to $i > 60^\circ$. We find eight galaxies that fit this criterion. This method works well for spirals of intermediate to late Hubble types, but does not capture all highly inclined disks for S0s because for some edge-on or highly inclined S0s, a rounder, thickened outer stellar component can sometimes dilute the outermost isophote so that the outermost ellipticity is below 0.5 although the galaxy is highly inclined.

Therefore, our second method is to visually identify highly inclined S0s. We visually identify these systems using the criteria that a thinner, high surface brightness, highly inclined disk appears embedded in a thick, diffuse stellar component, which could be a mix of thick disk, bulge, and bar stars. A typical example of one of these galaxies is shown in Figure 5. We encounter four such cases, where the galaxy appears visually to be close to edge-on and is classified as highly inclined. We distinguish these cases from a face-on galaxy with a bar because (1) the thin, highly inclined disk and the thicker stellar component are always oriented along the same PA, (2) the thick outer stellar component in these highly inclined S0 galaxies appears much fainter and more diffuse than a face-on disk, and (3) in three out of these four galaxies, a box or X-shaped bulge is present, suggesting that the galaxy is seen edge-on (e.g., Athanassoula 2005). We therefore exclude from further analysis the 12 highly inclined systems that we find in the sample.

3.2.2. Detecting Barred Galaxies

Traditionally, when ellipse fits are used to identify bars, a galaxy is classified as barred if the radial profiles of the ellipticity and PA fulfill the following requirements: (1) the e rises to a *global* maximum, $e_{\rm bar} > 0.25$, while the PA remains relatively constant (within $\pm 10^\circ$), and (2) the e drops by at least 0.1 and the PA changes by more than 10° at the transition between the bar and disk region. An example of a barred S0 galaxy in our sample that meets the traditional criteria is shown in Figure 6.

These criteria will identify primary stellar bars in the vast majority of spirals, particularly those of intermediate to late Hubble types (Sb–Sm). However, they can marginally fail in some galaxies due to a rare set of circumstances, which we describe in detail below. These circumstances are particularly likely to occur in S0s with large bulge-to-disk ratios.

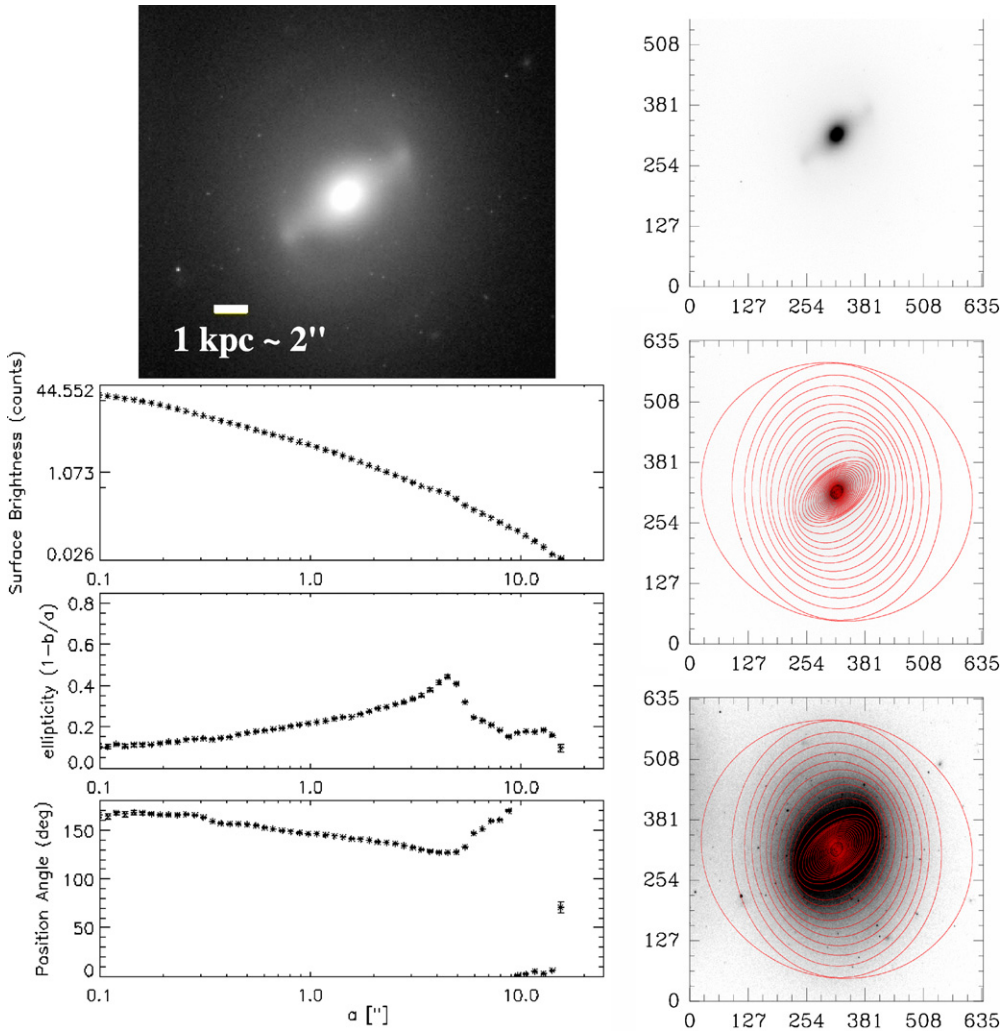

Figure 6. Left: *HST* image and radial profiles of surface brightness, e, and PA of a barred cluster galaxy. In this example, the traditional bar signature is evident in the smooth rise of the e to a global maximum of ∼0.4, while the PA remains relatively constant in the bar region. The e then drops and the PA changes, indicating the transition to the disk region. Right: the ellipse fits are overlaid onto the galaxy image. The top two panels are shown with a stretch that enhances the inner disk and bar regions, while the bottom panel shows the outer disk. See Section 3.2.2 for details.

(A color version of this figure is available in the online journal.)

In some S0s, a combination of structural parameters and viewing angle causes the observed (i.e., not deprojected) maximum bar ellipticity ($e_{\rm bar}$; typically measured from the isophote crossing the end of the bar) to become a *local* maximum of the ellipticity radial profile rather than the *global* maximum. In these rare cases, the ellipticity ($e_{\rm disk}$) of the outer disk becomes the *global* maximum in the radial profile of ellipticity. This can happen in the case of a barred galaxy, where all or most of the following conditions are satisfied: (i) the galaxy has a moderate to large inclination (e.g., $i > 50°$). This causes the outer circular disk of the galaxy to appear elongated along the line of nodes (LONs) in the projected image of the galaxy on the sky, leading to a higher measured $e_{\rm disk}$. (ii) A large fraction of the length of the bar lies within a fairly axisymmetric bulge, which is much more luminous than the bar. In this case, the bulge light dilutes the ellipticity of the bar by "circularizing" the isophote crossing the bar end, thus causing $e_{\rm bar}$, measured from this isophote to be significantly lower than the true ellipticity of the bar. (iii) The bar major axis has a large offset ($\Delta\theta$) with respect to the LON, such that projection effects make the disk appear more elongated, while the bar appears more round. The most extreme example occurs when the bar is perpendicular to the LON (i.e., $\Delta\theta = 90°$). Such situations can potentially cause the observed ellipticity of the disk to exceed that of the bar. Thus, a combination of factors (i) to (iii) can cause the measured $e_{\rm bar}$ to fall below $e_{\rm disk}$ so that $e_{\rm bar}$ is a *local* maximum in the e radial profiles. In this case, the bar can still be identified through ellipse-fits if the traditional criterion that the measured maximum bar ellipticity $e_{\rm bar}$ must be a *global* maximum is relaxed, and a *local* maximum be deemed acceptable.

In the case of barred S0s, the conditions (i) to (iii) can be satisfied in a larger fraction of galaxies than for a sample of barred intermediate-to-late Hubble type (Sb–Sm) spirals due to the following reasons. Many barred cluster S0s host bulges that are bright, have large bulge-to-disk light ratios, and encompass a large fraction of the length of the bar. Indeed, among our sample of 20 moderately inclined cluster S0s, we find three such cases and an example is shown in Figure 7. For this reason, we quote two bar fractions derived through ellipse fits: the first bar fraction ($f_{\rm bar,ES}$), where we use the strict criteria (1) and (2) above, and the second bar fraction ($f_{\rm bar,ER}$) where for galaxies satisfying (i) to (iii), we relax the criterion that the maximum bar ellipticity must be a *global* maximum (however we still require it to rise above $e = 0.25$). We note that all bars identified

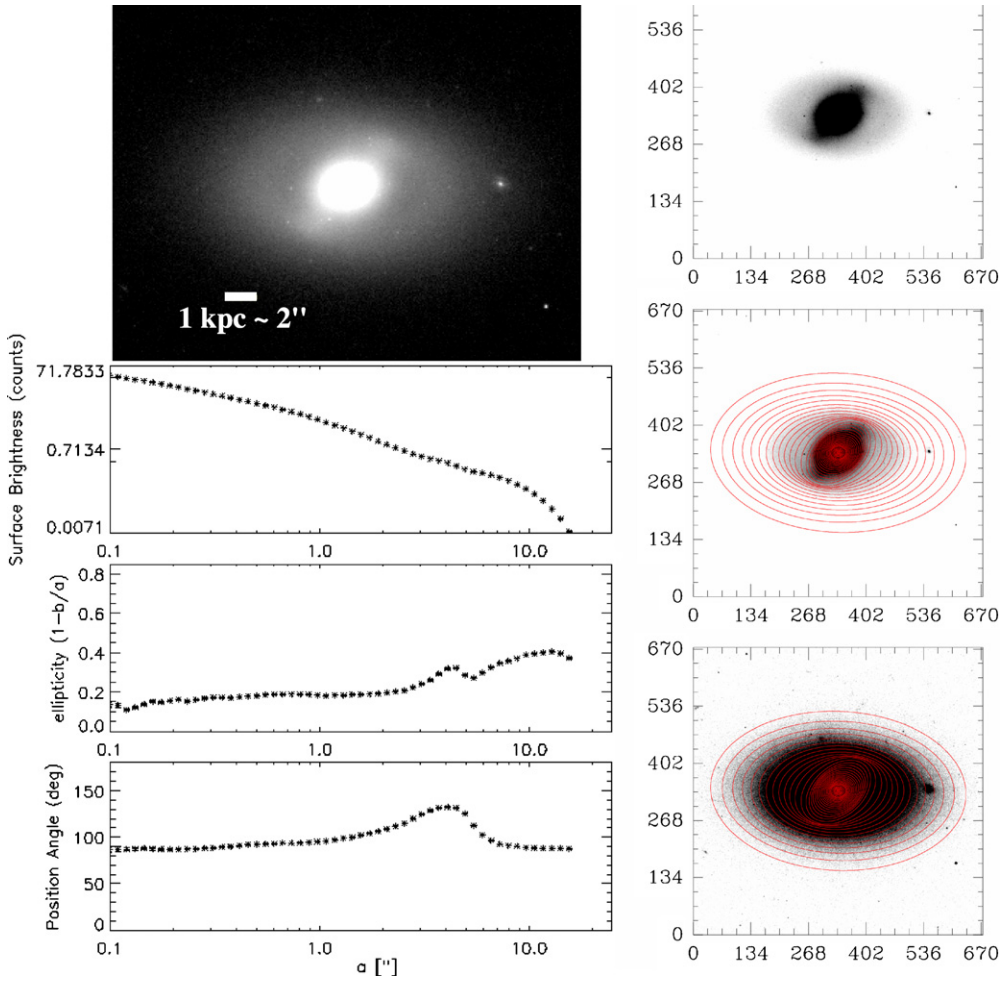

Figure 7. Panels are as in Figure 6, but here we show an example of a barred galaxy that does not meet the strict ellipse-fit criterion requiring that $e_{\rm bar}$ is the *global* maximum in the *e* radial profile. In this case, the observed outer disk ellipticity $e_{\rm disk}$ is higher than $e_{\rm bar}$, making it a *local* maximum in the *e* radial profile. This happens due to a combination of properties of the galaxy: (1) the galaxy is inclined ($i \sim 51^\circ$) causing the outer disk to be elongated along the line of nodes with a significant ellipticity ($e_{\rm disk} = 0.37$); (2) the stellar bar is significantly offset (by $\sim$45°) with respect to the line of nodes and hence its intrinsic axial ratio is diluted by projection effects; (3) the stellar bar has a significant fraction of its length inside a very luminous bulge, and the measured bar ellipticity is diluted to lower values than the true $e_{\rm bar}$. Therefore this galaxy is identified as "barred" through the relaxed ellipse-fitting criteria. We find three such cases among the bright Coma S0 galaxies (see Section 3.2.2).

(A color version of this figure is available in the online journal.)

with the strict ellipse-fitting criteria ("ES") are also picked up under the relaxed ellipse-fitting criteria ("ER"). We further note that, for the galaxies where the bar is detected only through the relaxed criteria, if the radial profiles of the ellipticity and PA are deprojected (Section 3.7), the bar ellipticity $e_{\rm bar}$ does become the global maximum. However, because many large studies of bars do not deproject the radial profiles (e.g., M09), we use the observed radial profiles to detect the bars as described above for ease of comparison.

3.3. Identification of Bars in S0s via Visual Classification

In addition to ellipse fitting, we also present the optical bar fraction for bright S0s in Coma from visual classification performed by I.M., S.J., and P.E. This facilitates comparison to other work where bars are identified visually (Section 3.5).

A galaxy is classified as "barred" through visual classification if it has a significant elongated feature extending from the center of the disk with an axial ratio (estimated from the image with *DS*9) <0.7 and a PA that differs from the PA of the outer disk by at least 10°. A galaxy is classified as "unbarred" if there is no elongated structure present that fits the above criteria.

All of the bright barred S0s we identify in the Coma sample through ellipse fitting and visual classification are listed in Table 1. The methods through which the bar is detected are shown in Column 5.

3.4. Optical S0 Bar Fraction in the Central Region of the Coma Cluster

The optical bar fractions for our sample of bright S0 galaxies in the Coma cluster core are presented in Table 2.

Using the strict ellipse fitting criteria (Section 3.2.2), we find that the optical bar fraction for the bright S0s is $f_{\rm bar,ES} = 50\% \pm 11\%$ (10/20). Using the relaxed ellipse fitting criteria, we find $f_{\rm bar,ER} = 65\% \pm 11\%$ (13/20). Visual classification gives an optical bar fraction of $60\% \pm 11\%$ (12/20). All errors are binomial errors. The barred S0 galaxies identified through ellipse fitting and visual classification are shown in Figure 8.

To correctly derive the bar fraction for S0s in clusters, we need to accurately estimate the number of unbarred S0s ($N_{\rm unbar}$ in Equation (1)). As S0s are devoid of typical disk features such as spiral arms, star-forming rings, etc., it is particularly challenging to *visually* identify all unbarred S0s and separate

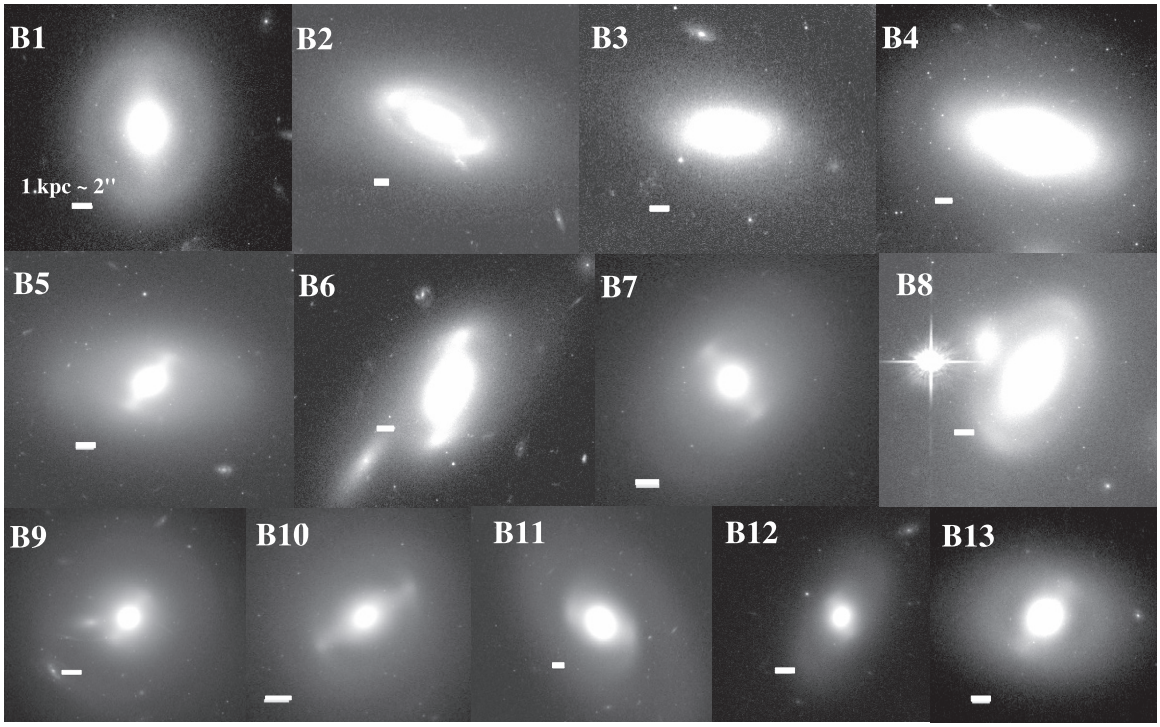

Figure 8. Barred bright ($M_V \lesssim -18$) S0 galaxies in the Coma cluster core found through ellipse fits (strict and relaxed criteria) and visual classification (see Section 3.2 and Table 1). All bars identified through the relaxed ellipse fit criteria are also identified by visual classification and vice versa. Bright stars such as the one in B8 are masked during the fitting.

Table 1
Optically Barred Bright ($M_V \lesssim -18$) S0s

Bar ID	Galaxy ID	R.A. (AB mag)	Decl.	$M_{I(814)}$	Bar Detection Method	e_{bar} obs	e_{bar} dep	a_{bar} obs (kpc)	a_{bar} dep (kpc)
(1)	(2)	(3)	(4)	(5)	(6)	(7)	(8)	(9)	(10)
B1	COMAi125710.767p272417.44	194.29486	27.404846	−20.1	ES, ER, V	0.35	0.26	2.97	2.99
B2	COMAi125833.136p272151.77	194.63806	27.364383	−20.0	ES, ER, V	0.68	0.54	3.19	3.52
B3	COMAi125928.728p28225.90	194.86970	28.040531	−19.7	ES, ER	0.49	0.40	2.26	2.44
B4	COMAi125929.956p275723.26	194.87481	27.956462	−21.1	ES, ER, V	0.47	0.51	4.36	5.04
B5	COMAi125946.775p275825.88	194.94490	27.973856	−20.6	ES, ER, V	0.39	0.70	2.22	2.82
B6	COMAi125956.707p275548.62	194.98628	27.930173	−19.9	ES, ER, V	0.55	0.46	3.42	4.00
B7	COMAi13022.156p28249.08	195.09231	28.046968	−20.6	ES, ER, V	0.37	0.46	1.92	2.23
B8	COMAi13038.731p28052.22	195.16137	28.014507	−20.3	ES, ER, V	0.47	0.31	3.57	3.77
B9	COMAi13042.753p275816.88	195.17814	27.971355	−21.3	ES, ER, V	0.25	0.31	1.46	1.55
B10	COMAi13042.833p275746.98	195.17846	27.963052	−20.3	ES, ER, V	0.43	0.46	2.48	2.64
B11	COMAi125930.825p275303.42	194.87843	27.884283	−21.1	ER, V	0.33	0.35	1.99	2.33
B12	COMAi13017.020p28350.10	195.07092	28.063917	−19.0	ER, V	0.29	0.40	1.14	1.45
B13	COMAi13027.971p275721.54	195.11654	27.955985	−20.1	ER, V	0.31	0.47	2.09	2.79

Notes. (1) Bar ID; (2) Galaxy ID as given in the Coma Treasury survey DR2 (Hammer et al. 2010); (3) R.A. (J2000); (4) Decl. (J2000); (5) $M_{I(814)}$ absolute magnitude in AB mag; (6) Bar detection method: "ES": strict ellipse fit criteria (Section 3.2.2), "ER": relaxed ellipse fit criteria (Section 3.2.2), and "V": visual classification on direct image (Section 3.3); (7) Observed peak bar ellipticity e_{bar}; (8) Deprojected peak bar ellipticity; (9) Observed bar semimajor axis a_{bar} measured at e_{bar}; (10) Deprojected bar semimajor axis (Section 3.7).

Table 2
Optical Bar Fraction for Bright ($M_V \lesssim -18$) S0s Based on Different Methods

Method	Unbarred	Barred	$f_{bar,opt}$
Ellipse fit, strict	10	10	50% ± 11%
Ellipse fit, relaxed	7	13	65% ± 11%
Visual classification	8	12	60% ± 11%

Notes. Optical bar fraction for the 20 moderately inclined ($i < 60°$) bright ($M_V \lesssim -18$) S0 galaxies. Barred galaxies are characterized through: (1) ellipse fitting using the strict criteria (where e_{bar} is required to be a global maximum in the ellipticity profile), (2) ellipse fitting using relaxed criteria (e_{bar} can be a local maximum), and (3) visual classification.

them from ellipticals. Therefore, in Section 3.1, we identified S0s through both visual classification and two-dimensional structural decomposition of the images into single-component Sérsic models, bulge+disk models, and bulge+disk+bar models. We found 13 Es, 32 S0s, and 1 E/S0 case, which still remains ambiguous even after decomposition. This ambiguous E/S0 case is not included in the optical bar fraction in Table 2. If it is included as an unbarred S0 in our analysis, the optical bar fractions fall to: $f_{bar,ES} = 48\% \pm 11\%$, $f_{bar,ER} = 62\% \pm 11\%$, and $57\% \pm 11\%$ from visual classification. We therefore estimate that the uncertainties associated with determining the

Table 3
Optical Bar Fraction for Bright ($M_V \lesssim -18$) S0s in Different Environments

Study	Environment	Number Density (galaxies Mpc^{-3})	Velocity Dispersion (km s^{-1})	S0 f_{bar} for $M_V \lesssim -18$
(1)	(2)	(3)	(4)	(5)
Bars identified through ellipse fitting (strict criteria; Section 3.2.2)				
This work	Coma central region, $z \sim 0.02$	10,000	900[a]	50% ± 11% (10/20)
M09[b]	A901/902 clusters, $z \sim 0.165$	1000	800–1200[c]	39% ± 5% (38/98)
E11	Virgo, $z \sim 0$	300	400–750[d]	44% ± 14% (12/27)
Bars identified through ellipse fitting (relaxed criteria; Section 3.2.2)				
This work	Coma central region $z \sim 0.02$	10,000	900	65% ± 11% (13/20)
M09[b]	A901/902 clusters, $z \sim 0.165$	1000	800–1200	48% ± 5% (47/98)
E11	Virgo, $z \sim 0$	300	400–750	48% ± 14% (13/27)
Bars identified through visual classification				
This work	Coma central region, $z \sim 0.02$	10,000	900	60% ± 11% (12/20)
T81[e]	Coma central region, $z \sim 0.02$	10,000	900	42% ± 7% (19/45)
M09[b]	A901/902 clusters, $z \sim 0.165$	1000	800–1200	55% ± 5% (54/98)
E11[f]	Virgo, $z \sim 0$	300	400–750	59% ± 9% (16/27)

Notes. T81: Thompson 1981; M09: Marinova et al. 2009; E11: P. Erwin et al. (2012, in preparation).
[a] The & White (1986).
[b] We use a sub-sample from M09, with the criteria outlined in Section 3.5.
[c] Heiderman et al. (2009).
[d] Binggeli et al. (1987).
[e] Bar classification is performed on ground-based KPNO plates.
[f] For this paper, visual classification is performed on the E11 sample by P.E., I.M., and S.J. using the criteria outlined in Section 3.3.

number of unbarred S0s can lead us to overestimate the optical bar fraction by only a small factor of ∼1.05.

We note that in the field, the bar fraction is lower in the optical than in the NIR by factor of 1.3 (Eskridge et al. 2000; M07) for intermediate (Sab–Sc) Hubble types due to obscuration by gas, dust, and star formation. However in S0s, where there is little gas and dust on large scales, we do not expect the difference between the optical and NIR bar fractions to be significant.

3.5. S0 Bar Fraction Across Different Environments

Due to the fact that different bar detection methods can yield different bar fraction results, it is important to compare studies using the same methods for consistency. In addition, as discussed in Section 1, the bar fraction depends on host galaxy properties such as Hubble type or B/T (Odewahn 1996; BJM08; Aguerri et al. 2009; M09; Weinzirl et al. 2009; Laurikainen et al. 2009), luminosity (Barazza et al. 2009; M09), stellar mass, and color (Nair & Abraham 2010a; Cameron et al. 2010). Therefore we use comparison samples that are matched as well as possible to our Coma sample in Hubble type (S0s), luminosity ($M_V \lesssim -18$), color, and method of bar detection. We compare our results for S0s to those of other studies in Coma and lower-density clusters (A901/902 and Virgo).

First, we compare to another study in the very dense environment of the central regions of the Coma cluster (galaxy number density $n \sim 10{,}000$ galaxies Mpc^{-3}) by T81. T81 uses visual classification on ground-based Kitt Peak National Observatory (KPNO) plates to detect bars in S0s brighter than $M_V = -17.5$ (very similar to our magnitude cutoff of $M_V \sim -18$). Therefore, we compare his result to our optical bar fraction from visual classification (Section 3.3). Table 3 shows that our optical bar fraction from visual classification for S0s (60% ± 11%) in the Coma core is higher than the result (42% ± 7%) that T81 obtained after correcting raw galaxy counts for projection effects.[18] A clue to the reason for this difference comes from our finding that in many S0s in our sample, the bar ellipticity and its overall signature are diluted because the bulge is bright compared to the bar and it is large enough to encompass a large fraction of the bar length. In such cases, as discussed in Section 3.2.2, the bar is harder to detect via any method, be it visual classification or ellipse fits, unless the image is of high quality and the classifier has significant expertise. In the case of T81, the visual classification was performed on ground-based optical plates, which are of lower quality than CCD images, making it even more difficult to detect such diluted or/and short bars. It is not possible to directly compare our case-by-case results with T81, as he does not publish the list of galaxies he classifies as barred and does not provide the lengths and ellipticities of the bars. However, we perform two indirect tests to gauge the impact of missing diluted, weak, and/or short bars. In our sample, seven of the 13 barred S0s have an observed peak bar ellipticity $e_{bar} < 0.4$ (Figure 12). If all of these galaxies were classified as unbarred, the bar fraction would drop to 30%. Alternatively, if the shorter ($a_{bar} < 2$ kpc) bars are excluded, the bar fraction would drop to 45%. These tests suggest that it is likely that the lower optical bar fraction of T81 is due to his missing some of these diluted or/and short bars.

For a comparison to intermediate-density cluster environments, we use the study of M09 for the A901/902 cluster system ($z \sim 0.165$; $n \sim 1000$ galaxies Mpc^{-3}, see Table 5 in Heiderman et al. 2009). To match our sample, we pick S0 galaxies from the M09 study with $M_V \leqslant -18$, using classifications performed by the members of the STAGES collaboration for the A901/902 cluster system (Gray et al. 2009; see Wolf et al. 2009 for more

[18] This correction is used by T81 to account for the effects of foreground and background objects contaminating the cluster field in the absence of spectroscopic data. Since all bright S0s in our Coma core sample are spectroscopically confirmed cluster members, we compare to the corrected bar fraction from T81.

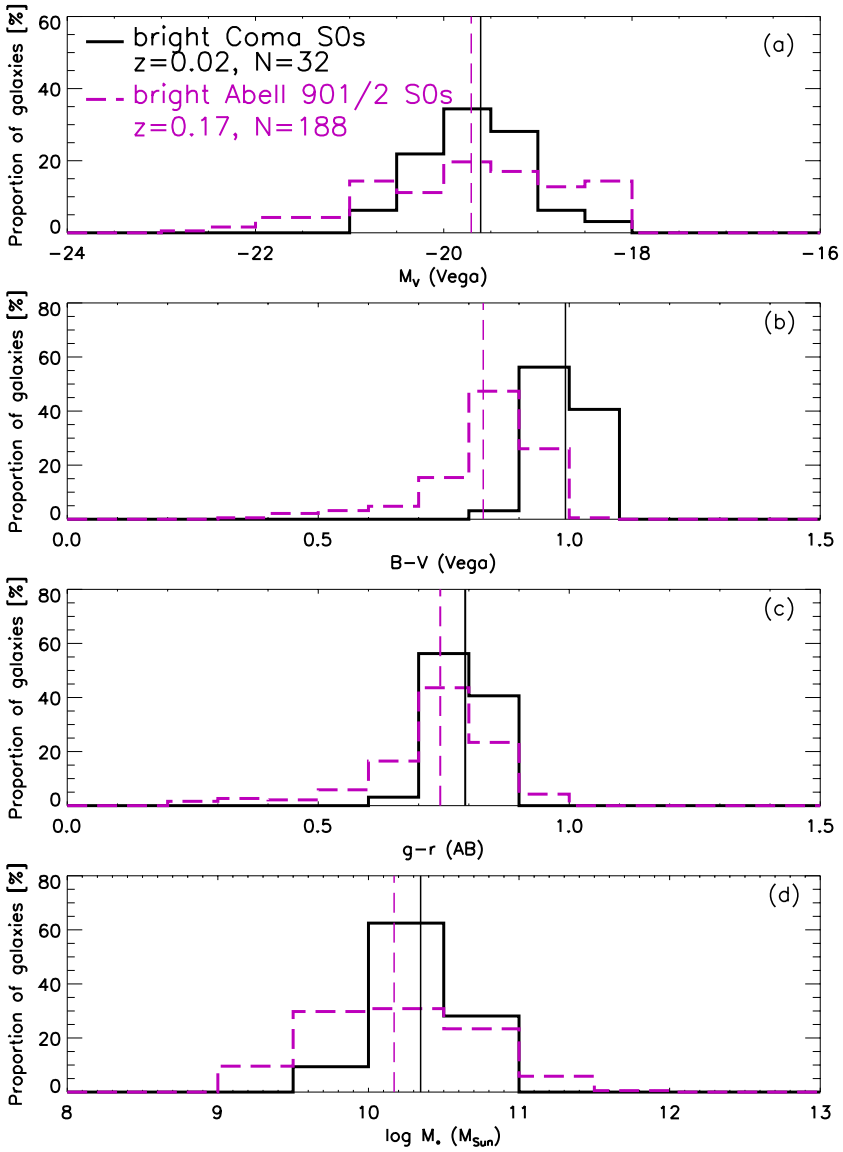

Figure 9. Properties of bright S0 galaxies in the A901/902 cluster system (dashed pink lines) and Coma (solid black line). The vertical lines show the mean values for each distribution. The two samples are well matched in mean luminosity, $g-r$ color, and stellar mass. However, the results of a Kolmogorov–Smirnov (K-S) test show differences in the overall distributions for $g-r$ color and stellar mass (K-S ($p = 0.002$, $D = 0.4$) and (0.005,0.3), respectively) and are inconclusive for the distributions of M_V (K-S ($p = 0.13$, $D = 0.2$)). This is likely due to the fact that the A901/902 sample has a tail of galaxies with masses both lower and higher than the Coma core sample, translating, respectively, into a tail of bluer colors and brighter absolute magnitudes. The A901/902 S0s appear ∼0.2 mag bluer in $B-V$ color, on average (K-S ($p = 6 * 10^{-16}$, $D = 0.8$)). We believe that this $B-V$ color offset is not real and is caused by the fact that the color transformations derived by Jester et al. (2005) for stars may not be adequate for S0s.

(A color version of this figure is available in the online journal.)

details). In M09, inclined galaxies were picked as those with outer disk ellipticity $e_{\rm disk} > 0.5$, as traditionally done in bar studies using ellipse fitting. However, since we are only focusing on S0 galaxies (which sometimes have large bulges/diffuse, thick stellar components that can dilute the $e_{\rm disk}$ below 0.5 even for edge-on S0s, as discussed in Section 3.2.1) we apply the same additional visual criteria outlined in Section 3.2.1 to the M09 S0 sample to detect and remove highly inclined S0s.

Figure 9 shows the host galaxy properties of the A901/902 and Coma S0 samples. The two samples are well matched in the *mean* luminosity, $g-r$ color, and stellar mass. However, the results of a Kolmogorov–Smirnov (K-S) test show differences in the overall distributions of $g-r$ color and stellar mass (K-S ($p = 0.002$, $D = 0.4$) and (0.005, 0.3), respectively), and are inconclusive for the distributions of M_V (K-S ($p = 0.13$, $D = 0.2$)). This is likely due to the fact that the A901/902 sample has a tail of galaxies with masses both lower and higher than the Coma core sample, translating, respectively, into a tail of bluer colors and brighter absolute magnitudes. Oddly, there appears to be a significantly larger offset between the A901/902 cluster and the Coma core if one uses the $B-V$ color (Figure 9(b)) rather than the $g-r$ color (Figure 9(c)): A901/902 S0s appear ∼0.2 mag bluer in $B-V$ color compared to the Coma core, and the K-S test suggests a large difference (K-S ($p = 6 * 10^{-16}$, $D = 0.8$)). However, we believe that this $B-V$ color offset is not real and is caused by the fact that the color transformations derived by Jester et al. (2005) for stars may not be adequate for S0s.

In M09 bars were detected on optical (*HST* ACS F606W) images via the strict ellipse-fitting criteria only. We therefore

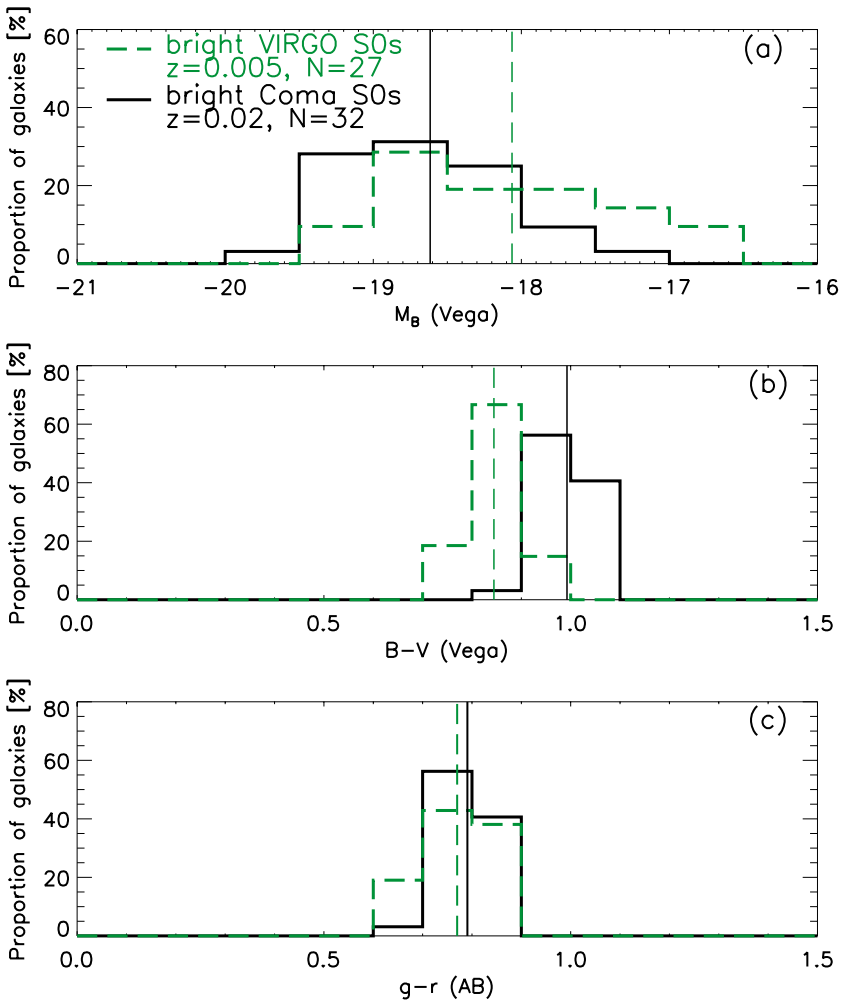

Figure 10. Properties of bright S0 galaxies in the Virgo cluster (dashed green line) and Coma (solid black line). The vertical lines show the mean values for each distribution. The two samples are well matched in mean luminosity and $g-r$ color. A K-S test shows differences in the overall distribution of M_B absolute magnitude ($p = 0.02$, $D = 0.4$), whereas the distributions of $g-r$ color are similar (K-S $p = 0.3$, $D = 0.3$). While the Virgo S0s appear bluer in $B-V$ (∼0.15 mag on average, with K-S ($p = 8 * 10^{-11}$, $D = 0.9$)) we believe that this color offset is not real since the measured $g-r$ colors (from SDSS in panel (c)) for the Coma and Virgo samples agree well. A possible reason for the offset in $B-V$ is that the color transformations derived by Jester et al. (2005) for stars may not be adequate for S0s.

(A color version of this figure is available in the online journal.)

also derive the bar fraction through visual classification and using the "relaxed" ellipse-fitting criteria for the S0s in the M09 sub-sample in order to derive the corresponding bar fractions for comparison to Coma S0s. As shown in Table 3, we find no statistically significant difference in the S0 bar fraction in A901/902 and Coma clusters when detecting bars through visual classification, strict ellipse fit criteria, or relaxed ellipse fit criteria. For instance, from visual classification (Table 3, bottom section), the Coma bar fraction (60% ± 11%) is slightly higher than the A901/902 bar fraction (55% ± 5%), but the difference is not statistically significant as the values are consistent within the error bars. Similarly, via the relaxed ellipse fitting criteria (Table 3, middle section), the Coma bar fraction is 65% ± 11%, while the A901/902 bar fraction is 48% ± 5%, (barely) consistent within the error bars. A comparison of the bar and disk properties (such as $e_{\rm bar}$ and $a_{\rm bar}/R_{25}$) in Coma and the A901/902 cluster system is discussed in Section 3.7.

Next, we compare to results in Virgo from P. Erwin et al. (2012, in preparation; E11). Virgo is the most nearby cluster ($D \sim 20$ Mpc, $z \sim 0.005$) and is representative of a low-density cluster environment ($n \sim 300$ galaxies Mpc^{-3} in the core region). We note however that different environmental tracers paint different pictures in Virgo. While the number density ($n \sim 300$ galaxies Mpc^{-3}) is lower than that of A901/902 ($n \sim 1000$ galaxies Mpc^{-3}) or the Coma core ($n \sim 10{,}000$ galaxies Mpc^{-3}), the velocity dispersions in Virgo can be as high as 750 km s^{-1} (Binggeli et al. 1987), comparable to those seen in A901/902 and much higher than in groups (∼100 km s^{-1}; Tago et al. 2008). These properties are relevant for the discussion of our results in Section 3.8. Our Virgo comparison sample consists of S0 galaxies brighter than $M_V = -18$ from E11. Figure 10(c) shows that the two samples agree well in $g-r$ color (K-S ($p = 0.3$, $D = 0.4$)), but Figure 10(b) shows that the $B-V$ colors of the Virgo S0s are significantly bluer (by ∼0.15 mag, on average, and with K-S values of ($p = 8 \times 10^{-11}$, $D = 0.9$)). We believe that this $B-V$ color offset between Coma and Virgo is not real since the measured $g-r$ colors for the two samples agree well. We again think this offset is likely caused by the possibility that the color transformations derived by Jester et al. (2005) for stars may not be adequate for S0s. We compare optical bar fractions derived with all three methods: strict ellipse fitting criteria (ES), relaxed ellipse fitting criteria (ER), and visual classification performed by P.E., I.M., and S.J. according to the criteria

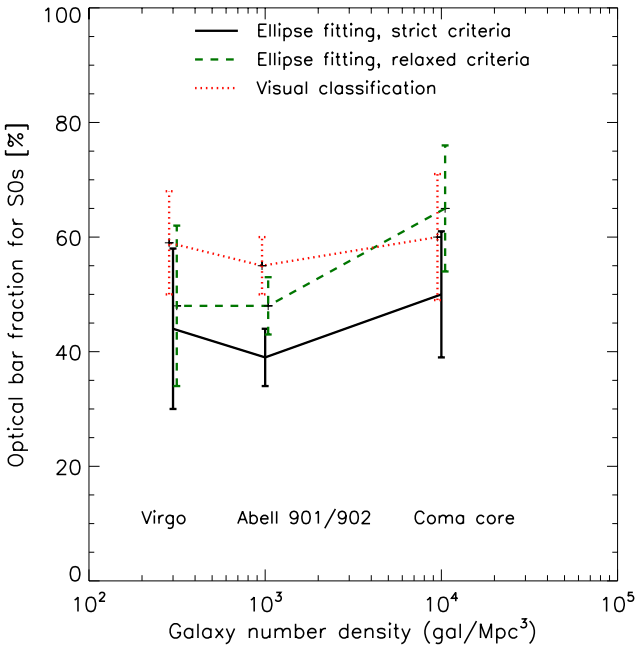

Figure 11. Optical bar fraction for S0 galaxies characterized through three methods (ellipse fitting with strict criteria, ellipse fitting with relaxed criteria, and visual classification) as a function of environment density. The different environments probed are the high-density core of Coma ($n \sim 10{,}000$ galaxies Mpc^{-3}), the intermediate-density A901/902 cluster system ($n \sim 1000$ galaxies Mpc^{-3}), and the low-density Virgo cluster ($n \sim 300$ galaxies Mpc^{-3}; Section 3.5). The bar fraction for S0s does not show a statistically significant variation across the environments probed, within the error bars.

(A color version of this figure is available in the online journal.)

outlined in Section 3.3. Again, we do not find a statistically significant difference in the optical bar fraction (within the errors) for S0s in the Coma core and those in Virgo using any of the three bar-detection methods above (see Table 3).[19]

A graphical representation of the trend of the bar fraction for S0s as a function of environment density is shown in Figure 11. We note that Figure 11 shows a hint of an increase in the mean bar fraction toward the dense core of the Coma cluster, however given the error bars, we cannot say whether this trend is significant. A comparison of the bar and disk properties for S0s in Coma and the Virgo cluster is discussed in Section 3.7.

We note that to compare to the lowest-density environments (i.e., field galaxies), we would ideally like to have a comparison sample where bar detection is done quantitatively via ellipse fits, and where the sample is matched to ours in both Hubble type (S0 galaxies), luminosity ($M_V \lesssim -18$), and color. However, there is as of yet no field comparison sample that fulfills all of the above requirements. The two large ellipse fit bar studies of field galaxies (BJM08 and Aguerri et al. 2009) are not adequate because they are mismatched in Hubble type and color (BJM08) or luminosity (Aguerri et al. 2009). Therefore, a comparison with these samples could be misleading, in light of recent results showing that the bar fraction varies non-monotonically with Hubble type, host galaxy luminosity, and color (Nair & Abraham 2010a). A comparison of the bar fraction derived through visual classification to a matched subset of S0s from the RC3 is complex, because RC3 galaxies are a mix of field and Virgo cluster members. The best candidate for a field comparison is the recently released public catalog by Nair & Abraham (2010b), containing visual morphologies for ∼14,000 SDSS galaxies. However, such a study is beyond the scope of this paper and therefore we defer this comparison to a later work.

Recently Méndez-Abreu et al. (2010) used the Coma Treasury survey data to analyze the properties of barred galaxies in the Coma cluster (using visual classification to detect bars). They do not select a disk sample but look for bars in all galaxies (including ellipticals and dwarfs). It is problematic and unconventional to quote the bar fraction from a sample of disk galaxies and ellipticals, particularly in the context of studying the bar fraction as a function of environment, as variations in this bar fraction can then be caused by the fact that the proportion of ellipticals to S0s to spirals changes strongly as a function of environment. For this reason, our study and other studies quote the bar fraction as the fraction of disk galaxies hosting bars. Comparison of our work with the results of Méndez-Abreu et al. (2010) is therefore not straightforward, but nonetheless we attempt a comparison to check whether our findings are consistent. If we include all galaxies from our sample in the magnitude range $-23 \leqslant M_r \leqslant -14$ to match their sample, we find a total (visual) bar fraction of $7\% \pm 2\%$ (14/188), while Méndez-Abreu et al. (2010) find 9% (secure bars) and 14% (weak/uncertain bars). Although our results are broadly consistent within the uncertainties, there are several further caveats to this comparison. Méndez-Abreu et al. (2010) apply the axial ratio constraint $b/a > 0.5$ to their whole sample, regardless of morphology, while we only apply an inclination cutoff to our bright disk galaxies. In addition to the inclination cutoff, we also exclude S0 galaxies deemed to be highly inclined/edge-on by eye, since as discussed in Section 3.2.1, using only the $i > 60^\circ$ cut misses highly inclined and edge-on S0s with a more circular, thickened stellar component. Furthermore, in the process of selecting cluster members, Méndez-Abreu et al. (2010) apply a color cut where they discard all galaxies that have $g - r$ color greater than 0.2 above their fit to the cluster red sequence.

3.6. Observed and Deprojected Properties

In Figure 12, we show the observed (solid line) and deprojected (dotted line) distributions of the bar semimajor axis ($a_{\rm bar}$) and bar ellipticity ($e_{\rm bar}$) for the 13 barred S0 galaxies detected through ellipse fitting (using both strict and relaxed criteria). In MJ07, we found that deprojecting the bar semimajor axis and ellipticity for a large sample makes only a very small statistical difference (a factor of 1.2), on average. However, since our Coma core sample is small, we deproject the observed radial profiles of ellipticity and PA and derive deprojected values of $e_{\rm bar}$ and $a_{\rm bar}$. We perform the deprojection using a code developed by Laine et al. (2002) and used previously in Laine et al. (2002), Jogee et al. (2002a, 2002b), and MJ07.

We find an observed mean bar size of 2.5 ± 1 kpc (2.9 ± 1 kpc deprojected; Figure 13) and the mean observed and deprojected bar ellipticity is 0.4 ± 0.1. It is evident that deprojection does not make a large difference in the mean $a_{\rm bar}$ and $e_{\rm bar}$. The observed and deprojected values of $a_{\rm bar}$ and $e_{\rm bar}$ of the three bars detected through the relaxed criteria only are shown as filled and open circles, respectively, in Figure 12. These galaxies satisfy the relaxed ellipse fit criteria, where the peak ellipticity of the bar is a local and not a global maximum due to the combination of factors discussed in Section 3.2.2. After deprojection removes the projection effects, which cause the ellipticity of the disk

[19] We note that Giordano et al. (2010) quote a much lower bar fraction (∼30%) using visual classification for Virgo S0 galaxies. This lower value is likely due to the fact that Giordano et al. (2010) include much fainter galaxies (down to $M_B = -15$), use a higher inclination cutoff ($i = 73^\circ$), and a different method for selecting cluster members.

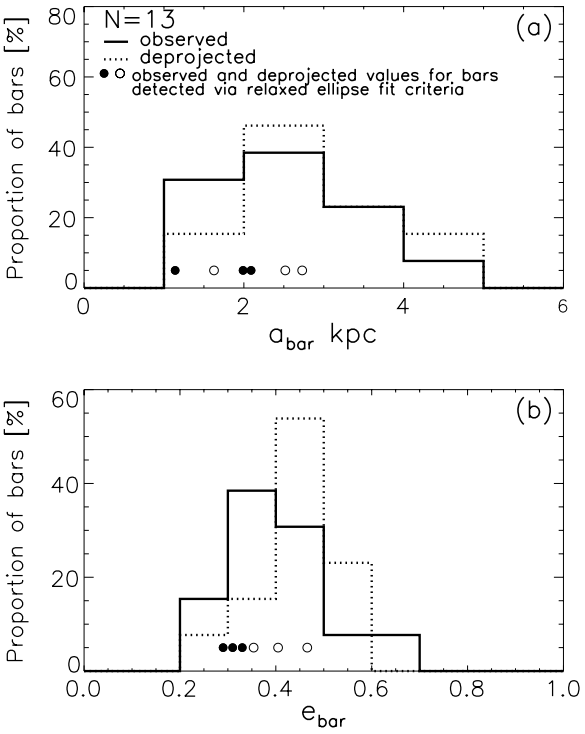

Figure 12. Observed (solid line) and deprojected (dotted line) bar size ($a_{\rm bar}$) (a) and ellipticity $e_{\rm bar}$ (b) distributions for the 13 barred S0 galaxies detected through ellipse fitting (including ones detected through relaxed criteria). The observed and deprojected values for the three bars detected through the ellipse fit relaxed criteria are shown as filled and open circles, respectively (Section 3.2.2). The mean observed $a_{\rm bar}$ for our barred S0s (including those detected with relaxed criteria) is 2.5 ± 1 kpc (2.9 ± 1 kpc deprojected), while the mean observed and deprojected $e_{\rm bar}$ is 0.4 ± 0.1. Most (85%) of bars have an observed $e_{\rm bar} \leqslant 0.5$. We also note that all extra bars that were detected via the relaxed ellipse fit criteria on the observed images would be detected via the strict ellipse fit criteria after deprojection. This is due to the fact that the latter removes projection effects, which cause the maximum bar ellipticity $e_{\rm bar}$ to go from a local maximum in the radial profile of ellipticity to a global maximum.

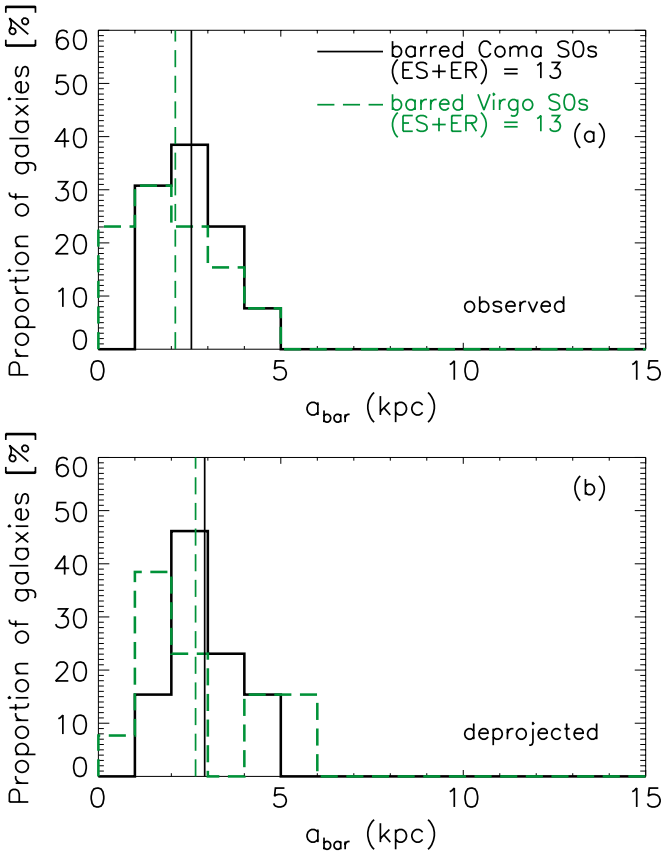

Figure 13. Comparison of the observed (a) and deprojected (b) bar semimajor axis $a_{\rm bar}$ distributions for our sample of barred bright Coma core S0s and those in Virgo from P. Erwin et al. (2012, in preparation). For both samples, the distributions include barred galaxies detected through the strict ellipse-fitting criteria as well as the relaxed criteria (Section 3.2.2). The vertical lines show the mean values for each distribution. We do not find a significant difference in the mean observed and deprojected bar size between Coma and Virgo S0s. The results from a K-S test are consistent with similar distributions (giving K-S ($p = 0.5$, $D = 0.3$) and (0.2, 0.4) for panels (a) and (b), respectively.

(A color version of this figure is available in the online journal.)

to be artificially boosted compared to the bar ellipticity, the peak bar ellipticity then becomes a global maximum in these three galaxies. Thus, after deprojection, these three barred galaxies also pass the strict ellipse fit criteria. The observed and deprojected $a_{\rm bar}$ for these galaxies are shorter than average. We note, however, that the bars of the three galaxies that failed to meet the strict ellipse fit criteria before deprojection are not necessarily weak bars. The intrinsic ellipticities $e_{\rm bar}$ of these three bars after deprojection are similar to the mean value of the whole sample (0.4 ± 0.1). This can be understood from the combination of factors discussed in Section 3.2.2, particularly the relative orientation of the bar with respect to the LON and projection effects.

Figure 13 shows that the mean observed and deprojected bar lengths ($a_{\rm bar}$) in our bright S0 Coma core sample are similar to those of S0s in the Virgo cluster (E11). The results from a K-S test are consistent with similar distributions (giving K-S ($p = 0.5$, $D = 0.3$) and (0.2, 0.4) for panels (a) and (b) of Figure 13, respectively). We explore the comparison of the bar and disk properties as a function of environment density in more detail below.

3.7. Properties of Disks and Bars in the Coma Core

We compare our sample of Coma cluster core S0s to the properties of S0s in less dense environments, namely, to those in the intermediate-density A901/902 cluster system ($z \sim 0.165$; M09) and those in the low-density Virgo cluster ($z \sim 0.005$; E11).

Figure 14 shows the distributions of (a) the galaxy disk R_{25} (the isophotal radius where $\mu_{\rm B}$ reaches 25 mag arcsec^{-2}); (b) bar semimajor axis $a_{\rm bar}$, measured at the peak bar ellipticity $e_{\rm bar}$ for all bars identified through ellipse fitting (ER+ES); (c) the $a_{\rm bar}/R_{25}$ ratio; and (d) peak bar ellipticity $e_{\rm bar}$ for the Coma, A901/902, and Virgo (E11) S0 samples. R_{25} values for the E11 Virgo sample are from the RC3. R_{25} for the Coma sample is estimated by ellipse fitting the galaxies on the ACS F475W images, which approximately correspond to SDSS g band. We calibrate the radial profiles of surface brightness to mag arcsec^{-2}, then convert them from $\sim g$ band (AB) to B mag arcsec^{-2} (Vega) using Equation (2). For two galaxies, we could not measure R_{25} radius because a good fit could not be obtained of the outer disk of the galaxy due to the presence of a close companion. For the M09 A901/902 sample, R_{25} is calculated from the absolute $M_{\rm B}$ magnitudes according to

$$\log\left(\frac{R_{25}}{\rm kpc}\right) = -0.249 \times M_{\rm B} - 4.00 \qquad (7)$$

from Schneider (2006). This formula is derived from an empirical relation measured for local spirals. To double-check its

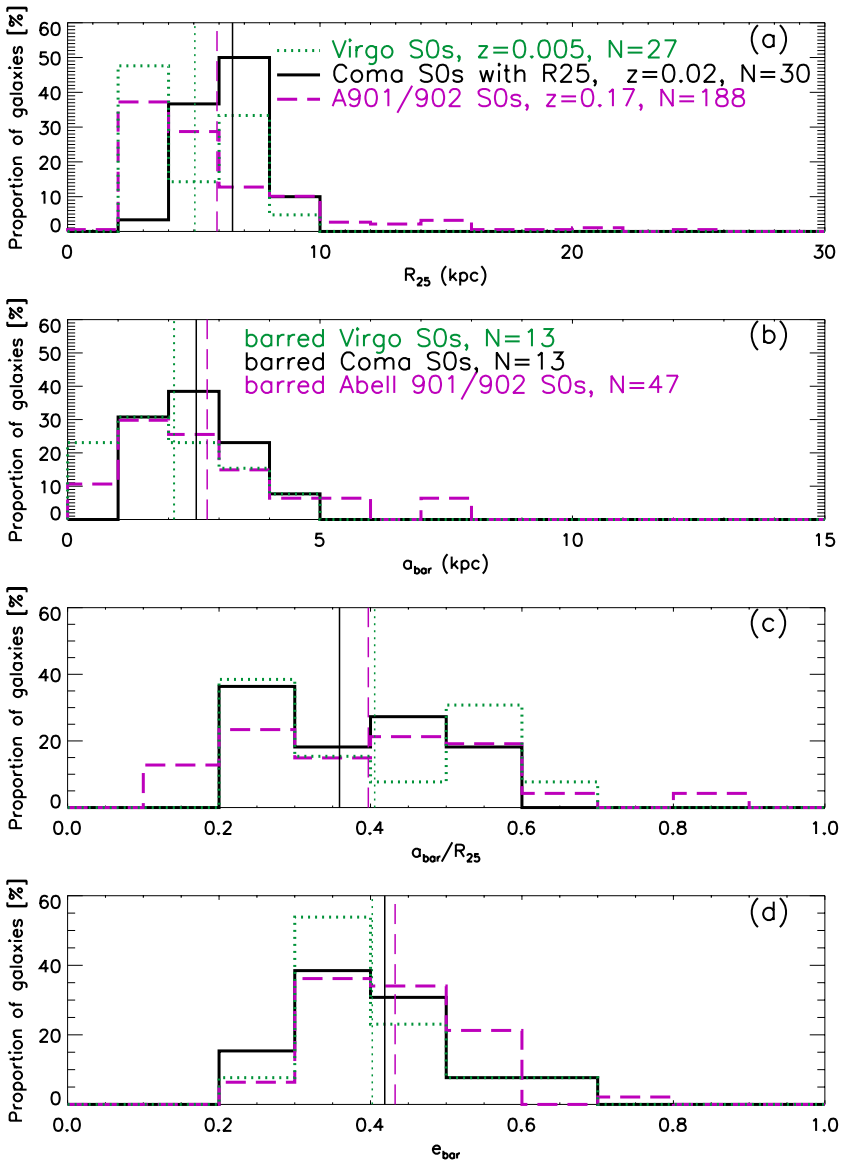

Figure 14. Distributions of (a) disk R_{25} (the isophotal radius where μ_B reaches 25 mag arcsec^{-2}), (b) bar semimajor axis a_{bar}, measured at the peak bar ellipticity e_{bar} for all bars identified through ellipse fitting (ER+ES), (c) a_{bar}/R_{25} ratio, and (d) peak bar ellipticity e_{bar} for the Coma S0 sample (solid black) and the comparison samples of S0s from the intermediate-density cluster system A901/902 (dashed pink) and the low-density Virgo cluster (dotted green). R_{25} values for Coma and A901/902 S0s are derived as described in Section 3.7, while R_{25} for Virgo galaxies are from the RC3. The vertical lines show the mean values for each distribution. All three samples have similar mean bar and disk properties, but the bar semimajor axis and disk R_{25} distributions for A901/902 S0s have a tail to larger values. The K-S statistic reflects the differences in the Coma, STAGES, and Virgo distributions of R_{25}, giving ($p = 0.008$, $D = 0.5$) between Coma and Virgo and ($p = 10^{-4}$, $D = 0.4$) between Coma and A901/902.

(A color version of this figure is available in the online journal.)

validity, we use it to calculate R_{25} radii for the Virgo S0s, where we already know R_{25} from RC3. Comparing the calculated values with those from RC3 confirms that the measured values from RC3 do follow the above relation, however it underpredicts the true R_{25} by ∼1.6 kpc on average. All three samples have similar mean bar and disk properties, but the bar semimajor axis and disk R_{25} distributions for A901/902 S0s have a tail to larger values. This tail corresponds to the tail of brighter S0s present in the A901/902 sample. The mean values of R_{25} for the Coma, A901/902, and Virgo S0s are 6.5 ± 1.3 kpc, 5.9 ± 2.8 kpc, and 5.0 ± 2.0 kpc, respectively. The K-S statistic reflects these differences in the Coma, STAGES, and Virgo distributions giving ($p = 0.008$, $D = 0.5$) between Coma and Virgo and ($p = 10^{-4}$, $D = 0.4$) between Coma and A901/902. The A901/902 and Virgo S0s have similar mean a_{bar}/R_{25} ratios of ∼0.4 ± 0.16, although the range in values is large (∼0.1–0.9). The K-S statistic is consistent with similar distributions, giving ($p = 0.9$, $D = 0.2$) and (0.6, 0.3) between Coma and A901/902 and Coma and Virgo, respectively. Coma S0s have a slightly lower mean $a_{bar}/R_{25} = 0.35 \pm 0.12$. An a_{bar}/R_{25} ratio of ∼0.3 ± 0.2 has also been found for field galaxies averaged over all Hubble types (e.g., MJ07; Menéndez-Delmestre et al. 2007) and for S0 galaxies (Erwin 2005). We note that the range of a_{bar}/R_{25} spanned by the three samples is quite large (∼0.1–0.9), however although our number statistics are small, this range is similar to that found for local field galaxies in MJ07.

All three samples have very similar distributions in bar ellipticity (K-S $p \sim 0.9$ and $D \sim 0.2$). The observed bar ellipticities we find for S0s in the Coma cluster as well as those

for S0s in Virgo and A901/902 are skewed toward lower values (e.g., mean $e_{\rm bar} \sim 0.3$–0.4) compared to the bar ellipticities in samples dominated by intermediate- to late-type galaxies (e.g., MJ07; BJM08; mean $e_{\rm bar} \sim 0.5$–0.7). This difference could be intrinsic (i.e., the bars in S0 galaxies are really less elliptical than those in later Hubble types) or it could be due to the dilution by the bright bulges of the isophotes crossing the end of the bar, where the ellipticity is measured (see Section 3.2.2). This effect has been demonstrated by Gadotti (2008).

3.8. Discussion: Implications for the Evolution of S0 Bars and Disks as a Function of Environment Density

What do our results imply for the evolution of bars and disks in bright S0 galaxies as a function of environment? We first recapitulate our results. Using three detection methods (traditional ellipse fit criteria, relaxed ellipse fit criteria, and visual classification), we found an optical bar fraction of $50\% \pm 11\%$, $65\% \pm 11\%$, and $60\% \pm 11\%$, respectively for our sample of bright ($M_{\rm V} \lesssim -18$) S0 galaxies in the central region of the Coma cluster (Section 3.4). We find that the bar fraction and properties (e.g., $e_{\rm bar}$, $a_{\rm bar}$) *in bright S0 galaxies* derived through all three of the above methods do not show a statistically significant variation (greater than a factor of ∼1.3) between the dense central regions of Coma ($n \sim 10{,}000$ galaxies Mpc^{-3}), the intermediate-density A901/902 clusters at $z \sim 0.165$ ($n \sim 1000$ galaxies Mpc^{-3}), and the low-density Virgo cluster ($n \sim 300$ galaxies Mpc^{-3}; Table 3). We note that there is a hint that the mean bar fraction may show a slight increase as a function of environment density toward the dense core of the Coma cluster (Figure 11), however given the error bars, we cannot say whether this trend is significant. Below, we explore what our results may imply for the formation and evolution of bars.

It has long been known that DM halo properties influence bar formation and evolution. At high redshifts (e.g., $z \sim 5$–8), recent theoretical studies of galaxy evolution using cosmological initial conditions find that bars are triggered by the triaxiality of DM halos and the asymmetric DM distribution as a whole (Romano-Díaz et al. 2008; Heller et al. 2007). These early bars are gas rich and quickly decay. Subsequent bar generations form and are destroyed during the major-merger epoch (e.g., $z \sim 2$–4) due to the rapidly changing potentials and gas dissipation associated with major mergers (Romano-Díaz et al. 2008). Although DM halos at early times can trigger bar formation due to their triaxiality, this triaxiality is diluted as disks and other central components form. The DM halos become more symmetric on a timescale that is a function of mass (e.g., Dubinski 1994; Kazantzidis et al. 2004; Heller et al. 2007). By $z \sim 1$ disks have also become more massive and stable. Simulations find that large-scale stellar bars forming at around this epoch are long-lived (Romano-Díaz et al. 2008; Heller et al. 2007). Interestingly, new observational results find that the bar fraction for the most massive disks ($M_* > 10^{11}\,M_\odot$) does not change between $z \sim 0.6$ and 0.2 (Cameron et al. 2010). However, the picture is complicated by the fact that for intermediate-mass disk galaxies ($M_* = 10^{10.5}$–$10^{11}\,M_\odot$), the bar fraction builds up by a factor of two over that redshift range. In addition, at $z \sim 0$, the bar fraction and properties are a non-monotonic function of the host galaxy properties, such as stellar mass, luminosity, color, Hubble type, and SF history (BJM08; M09; Aguerri et al. 2009; Barazza et al. 2009; Weinzirl et al. 2009; Laurikainen et al. 2009; Gadotti 2011; Nair & Abraham 2010a).

The picture above does not directly discuss environmental effects. In fact, there are still few theoretical and observational studies addressing this aspect of bar evolution. However, increasingly the emerging picture is suggesting that the frequency and properties of bars do not appear to be a sensitive function of environment (van den Bergh 2002; Aguerri et al. 2009; M09; Barazza et al. 2009; Cameron et al. 2010; although see Giuricin et al. 1993; Elmegreen et al. 1990).

How do the above results make sense in light of many theoretical studies that show that galaxy interactions can trigger bars in unbarred galaxies (e.g., Noguchi 1988; Mihos & Hernquist 1996)? We present a tentative picture below, considering the competing effects present in galaxy clusters. If a disk galaxy is sufficiently dynamically cold (i.e., Toomre $Q \lesssim 1.5$), it is susceptible to non-axisymmetric $m = 2$ instabilities (e.g., bars) whether spontaneously induced (e.g., Toomre 1981; Binney & Tremaine 1987) or tidally induced (e.g., Noguchi 1988; Hernquist 1989; Heller & Shlosman 1994; Mihos & Hernquist 1996; Jogee 2006, and references therein). The effect of the interaction depends on the geometry (i.e., prograde or retrograde encounter), with retrograde encounters having little to no effect on an already existing bar (e.g., Gerin et al. 1990; Steinmetz & Navarro 2002; Romano-Díaz et al. 2008; Aguerri & González-García 2009).

At $z < 1.5$, as clusters assemble and field galaxies fall into the existing cluster potential, let us now ask how the fraction and properties of bars in S0s might be expected to differ from the field environment. In a rich cluster, where the projected galaxy number density (n) and galaxy velocity dispersion (σ) is high, the timescale for close interactions (or collision timescale, $t_{\rm coll}$) will be short. We can estimate this timescale using

$$t_{\rm coll} = \frac{1}{n \sigma_{\rm gal} A}, \tag{8}$$

where n is the galaxy number density, $\sigma_{\rm gal}$ is the galaxy velocity dispersion, and A is the cross-section for close interactions defined as

$$A = \pi f (2 r_{\rm gal})^2. \tag{9}$$

We assume that f is unity, $r_{\rm gal} \sim 10$ kpc. For the Coma core $\sigma_{\rm gal} \sim 900$ km s^{-1} and $n \sim 10{,}000$ galaxies Mpc^{-3} (The & White 1986) giving a short timescale for close interactions $t_{\rm coll} \sim 90$ Myr.

However, although these close galaxy–galaxy interactions are frequent in a rich cluster, the large galaxy velocity dispersions present mean that each single encounter will be a *high-speed one*. Unlike single slow, strong encounters, a single high-speed encounter will typically not induce a large amount of tidal damage and not lead to major mergers. As a result, three factors may make it difficult for new bars to be induced in disk galaxies in a cluster. First, single high-speed encounters may not be as effective in inducing bars as slow, strong encounters, because the timescale over which gravitational torques act is short. Second, over time, the cumulative effect of many high-speed and weak encounters (galaxy harassment) can tidally heat disks (e.g., Moore et al. 1996; Aguerri & González-García 2009), making such disks dynamically hot (with Toomre $Q > 1.5$), and thus less susceptible to bar instabilities. Finally, in a cluster environment, the accelerated star formation history (e.g., Balogh et al. 2004, Blanton et al. 2005; Hogg et al. 2003) as well as physical processes such as ram pressure stripping (Gunn & Gott 1972; Larson et al. 1980; Quilis et al. 2000) will make S0 disks gas-poor, thus making them less bar-unstable. We therefore speculate that these three factors, namely, the predominance

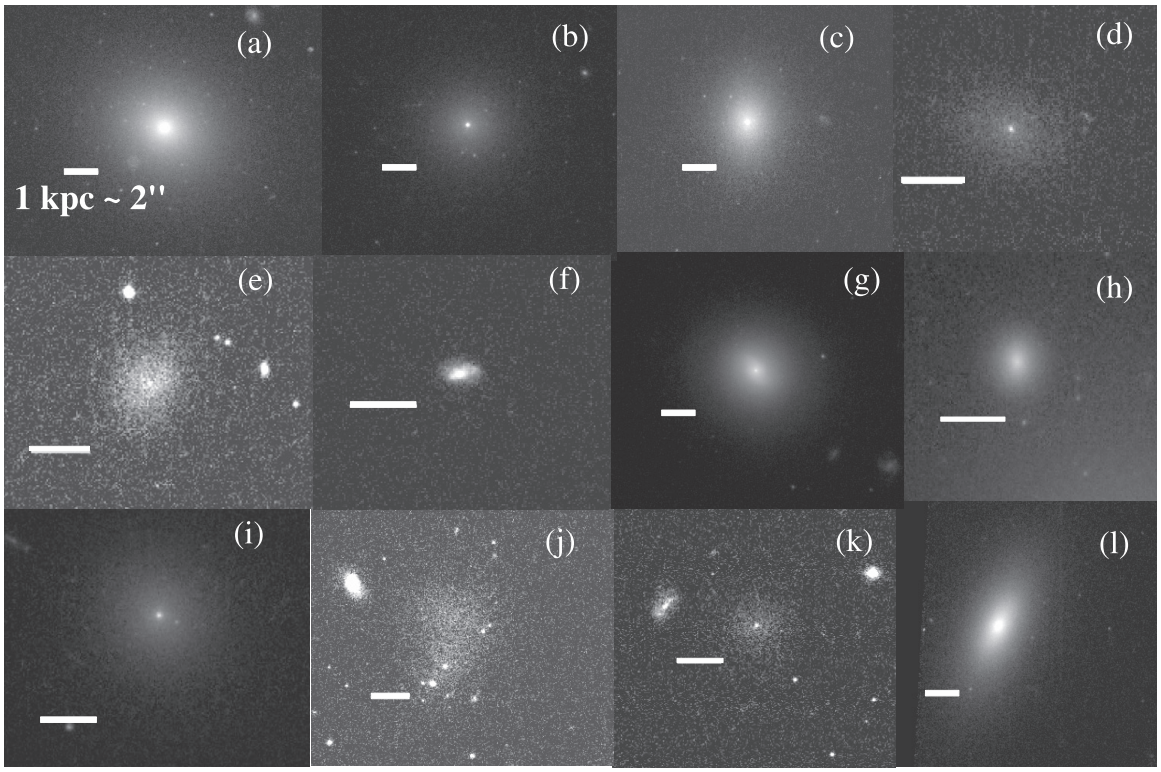

Figure 15. Examples of some of the faint, low-mass dwarfs in the Coma core sample. The scale bars are 1 kpc. The galaxies shown are: (a) COMAi13011.143p28354.92, (b) COMAi13025.977p28344.68, (c) COMAi13026.152p28032.02, (d) COMAi13029.853p28400.85, (e) COMAi13030.027p28135.08, (f) COMAi13039.068p28437.52, (g) COMAi13041.192p28242.38, (h) COMAi13047.670p28533.95, (i) COMAi13048.045p28557.42, (j) COMAi13050.590p28356.56, (k) COMAi13052.942p28435.86, (l) COMAi13030.949p28630.18.

of high speed encounters over slow ones, the tidal heating of S0 disks, and the low gas content of S0s in rich clusters, make it difficult for many new bars to be induced in S0 disks as they infall from a field-like to a cluster-like environment. This scenario may explain, at least in part, our findings that there is no strong variation in the optical bar fraction of S0s across the range of low density to high-density environments characterized by Coma, Virgo, and A901/902 in our study, as well as claims by other studies that there is no difference in the bar fraction between clusters and the field (van den Bergh 2002; Aguerri et al. 2009; Barazza et al. 2009; M09). Our interpretation for the result that the bar fraction is not greatly enhanced in the dense Coma cluster is also in agreement with that of Méndez-Abreu et al. (2010).

We note that it is possible that in rich clusters, the above effects, particularly the tidal heating, may cause existing bars to weaken. However, this effect is hard to robustly demonstrate observationally as the measured bar ellipticity is diluted by relatively large bulges in S0s (which dominate the disk population in clusters), while in the field, the disk population is dominated by spirals where such a dilution is not as severe (see Section 3.7).

It is also important to note that the arguments above, which explain why the bar fraction might not be greatly enhanced in rich clusters compared to the field, would lead to a rather different prediction for how the bar fraction in groups would compare to that in the field. In a group, the number density is moderately high ($n \sim 10$) but the galaxy velocity dispersions are typically low ($\sigma \sim 100$; Tago et al. 2008). Therefore slow, strong encounters are expected to be frequent in groups. Such encounters are likely to induce extra bars in disk galaxies compared to the field, particularly given the fact that the disks will not be stripped of their cold gas in groups as they would in rich clusters. In this context, we note that indeed higher bar fractions have been reported for early-type galaxies in binary pairs (Elmegreen et al. 1990) and early-type galaxies that are disturbed/interacting (Varela et al. 2004).

4. BARS AND DISK FEATURES IN COMA DWARFS

In addition to investigating bars in high-mass galaxies, we also take advantage of the exquisite resolution of the ACS (~50 pc at the distance of Coma) to search for bars and other disk features (e.g., spiral arms, edge-on disks) in the numerous dwarf galaxies in the central regions of the Coma cluster. Are some of these galaxies the remnants of late-type spirals that have gone through processing in a dense cluster environment? In Virgo, some early-type dwarfs are known to host features (e.g., lenses, bars, spiral arms; Sandage & Binggeli 1984; Binggeli & Cameron 1991; Jerjen et al. 2000; Barazza et al. 2002; Lisker et al. 2006, 2007; Lisker & Fuchs 2009) suggesting the presence of a disk. Not only can such features provide clues to the formation history of these systems, but the presence or absence of bar structures has implications for the conditions necessary for bar formation and growth in galaxies (e.g., Méndez-Abreu et al. 2010).

4.1. Identifying Dwarf Galaxies

As outlined in Section 2, we use a magnitude cut at $M_{I(814)} = -18.5$ (AB mag), (roughly corresponding to $M_V = -18$ Vega mag) to separate dwarf and normal galaxies. A montage of some of the faint, low-mass dwarfs in our Coma core sample is shown in Figure 15. Figure 16(a) shows the distribution of absolute magnitude $M_{I(814)}$ of the galaxies in the faint dwarf sample. Figure 16(b) shows where the dwarf galaxies lie on a plot of

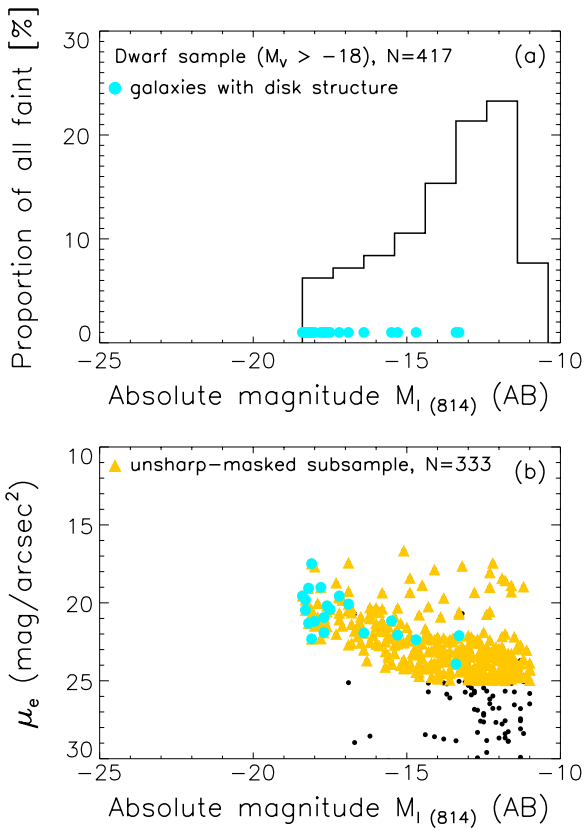

Figure 16. (a) Absolute magnitude ($M_{I(814)}$) distribution and (b) plot of surface brightness vs. absolute magnitude ($M_{I(814)}$) of the 417 galaxies in the Coma faint sample. The cyan points show the values for the 21 faint galaxies where we find disk structure (bar, spiral, edge-on disk) through unsharp masking. Most (76%) of the objects where we find disk structure have $M_{I(814)} \leqslant -16$.

(A color version of this figure is available in the online journal.)

the μ_e (the surface brightness at R_e) versus absolute magnitude $M_{I(814)}$. Effective radii and μ_e are from Hoyos et al. (2011), derived through single-component Sérsic fits.

Prior to applying the unsharp masking technique (Section 4.2) on the dwarf sample, we pick out good candidates through a cut in surface brightness ($\mu_e < 25$ mag arcsec^{-2}) and radius ($R_{90} > 100$ pc). These cuts remove very low surface brightness objects and those where we are unlikely to resolve disk structure. We choose a size cut at $R_{90} > 100$ pc, which is twice the ACS PSF at the distance of Coma. Out of the 417 dwarf galaxies, we find 333 dwarfs that satisfy these criteria. The μ_e versus $M_{I(814)}$ distribution of these galaxies is plotted with yellow triangles in Figure 16(b).

4.2. Identifying Bars and Other Disk Features in Dwarfs

In many dwarf galaxies disk features may not be readily apparent by eye (or traditional quantitative methods such as ellipse fitting) because their amplitude is very low and is overwhelmed by the smooth light from the galaxy. Which method is sensitive enough to detect faint spiral/bar structure in such systems? Jerjen et al. (2000) used residuals from subtracting the azimuthally averaged light profile of the galaxy from the original image to discover hidden spiral features in IC 3328 with deep Very Large Telescope (VLT) observations. They analyzed the spiral structure using Fourier expansion, finding that the amplitude of the spiral is only ∼3%–4%. However, upon further analysis of a larger sample of 20 Virgo dwarfs, Barazza et al. (2002) find that some spiral or bar-resembling residuals may be artifacts from the combination of the increasing ellipticity and twisting isophotes (due to triaxiality) present in these galaxies and not actual spiral structure. Fourier decomposition is similarly unsuccessful in many galaxies. Barazza et al. (2002) find that a much better method seems to be unsharp masking (e.g., Schweizer & Ford 1985; Mendez et al. 1989; Buta & Crocker 1993; Colbert et al. 2001; Erwin & Sparke 2003). In this method, no assumptions about the light profile/inclination of the galaxy are necessary. Recently, Lisker et al. (2006) also successfully employed unsharp masking on ∼470 Virgo dwarfs to look for evidence of bar/spiral structure. Graham et al. (2003) discovered two dwarf galaxies with spiral structure in the Coma cluster using unsharp masking as well as subtracting a symmetrical model to reveal non-symmetrical disk features (one of these galaxies is COMAi125937.988p28003.56 in Table 4, while the other is not covered by the Coma ACS Treasury survey). Chilingarian et al. (2008) use unsharp masking to find disk features in dwarf galaxies in A496. We therefore use the unsharp masking method to seek out bar (or spiral) structures in the Coma cluster core dwarf sample.

We perform unsharp masking for the 333 dwarf galaxies that fit the criteria outlined in Section 4.1. First, we smooth the galaxy images by convolving with a Gaussian using the IRAF task *GAUSS*. Then we divide the original galaxy image by the smoothed image. We choose the Gaussian smoothing kernel size to be ∼25 pixels, corresponding to ∼625 pc for our galaxies. We also try a range of smoothing lengths from ∼15 to 45 pixels (∼375–1125 pc) for a subsample of the galaxies and find no substantial change in the results. A point made by Lisker et al. (2006) is that in some cases, it is desirable to use an elliptical smoothing aperture matched to the outer ellipticity and PA of the galaxy, in order to avoid spurious detections that resemble an edge-on disk. For this reason, in all cases where we suspect that the galaxy host an inclined/edge-on disk, we also perform the unsharp masking using an elliptical PSF to ensure that the structures found are not spurious detections.

We find bars and/or spiral arms in 13 galaxies out of the 333 dwarfs in the unsharp-masked subsample. An additional eight galaxies show evidence of an inclined disk (or ambiguous inclined disk or bar). The galaxies where we find structure are listed in Table 4. Figure 17 shows examples of the residuals due to different types of structures: (a) spiral arms only, (b) bar and spiral arms, (c) inclined disk, (d) bar and/or spiral, and (e) ambiguous bar or inclined disk embedded in a stellar halo. The galaxies with disk structure are overplotted as cyan points in Figure 16. Most (76%) of the galaxies where we find disk structure are brighter than $M_{I(814)} = -16$ (AB mag). We discuss the possible implications of these results below.

4.3. Discussion: Barred Dwarf Galaxies in the Coma Core

Using visual inspection and unsharp masking we find only 13 galaxies with bars and/or spiral arms in our Coma core dwarf subsample of 333 galaxies with $\mu_e < 25$ mag arcsec^{-2} and $R_{90} > 100$ pc. Does this result imply that faint/dwarf galaxies with disks are very rare within the Coma population or rather that any existing disks in these galaxies are too dynamically hot to be unstable to disk instabilities?

Studies have long been finding early-type dwarf galaxies with spiral/bar structure in Virgo and Fornax (e.g., Sandage & Binggeli 1984; Binggeli & Cameron 1991; Jerjen et al. 2000; Barazza et al. 2002; Lisker et al. 2006, 2007; Lisker & Fuchs

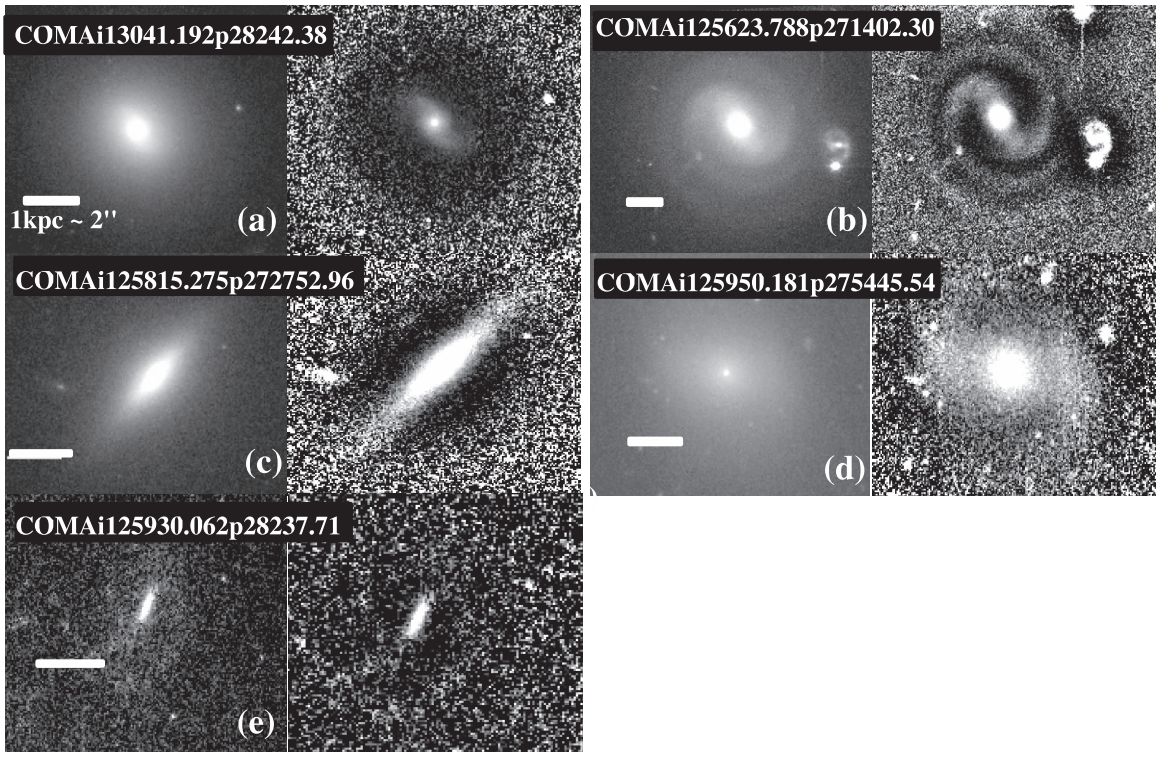

Figure 17. Examples of five galaxies from the dwarf ($M_V > -18$) sample highlighting the different types of disk structure that we find through unsharp masking: (a) spiral arms, (b) bar+spiral arms, (c) edge-on disks, (d) bar and/or spiral structure, and (e) ambiguous bar/edge-on disk (Section 4.2). We use a Gaussian smoothing kernel size of ~25 pixels, corresponding to ~625 pc at the distance of Coma. The original *HST* images are shown in the left panels and the corresponding residuals highlighting the disk structure are on the right. The scale bars show 1 kpc.

Table 4
Galaxies in the Faint ($M_V > -18$) Sample Where We Find Disk Structure Through Unsharp Masking

Galaxy ID (1)	R.A. (2)	Decl. (3)	Visit (4)	$M_{I(814)}$ (5)	Structure (6)
COMAi13030.949p28630.18	195.12895	28.10838	02	−17.6	inclined disk
COMAi13041.192p28242.38	195.17163	28.04510	08	−17.8	spiral
COMAi13018.883p28033.55	195.07867	28.00931	09	−18.1	bar
COMAi13013.398p28311.81	195.05583	28.05328	10	−17.7	inclined disk
COMAi13007.727p28051.91	195.03219	28.01441	10	−13.3	inclined disk
COMAi125930.062p28237.71	194.87525	28.04380	13	−13.4	bar/inclined disk
COMAi125904.792p28301.21	194.76997	28.05033	14	−18.3	bar
COMAi125911.545p28033.38	194.79811	28.00927	14	−18.2	inclined disk
COMAi125953.930p275813.76	194.97471	27.97048	18	−16.9	spiral
COMAi125937.988p28003.56	194.90827	28.00098	19	−18.0	bar + spiral
COMAi13035.418p275634.05	195.14758	27.94279	22	−17.7	bar
COMAi13024.823p275535.89	195.10342	27.92663	23	−18.2	bar + spiral
COMAi125950.181p275445.54	194.95909	27.91265	25	−17.5	bar
COMAi125820.533p272546.03	194.58555	27.42945	45	−18.3	spiral
COMAi125815.275p272752.96	194.56364	27.46471	45	−17.2	inclined disk
COMAi125814.969p272744.81	194.56237	27.46244	45	−15.5	bar + spiral
COMAi125825.308p271200.04	194.60545	27.20001	59	−18.4	bar + spiral
COMAi125623.788p271402.30	194.09912	27.23397	63	−18.1	bar + spiral
COMAi125638.099p271304.09	194.15875	27.21780	63	−16.4	bar
COMAi125845.297p274650.75	194.68873	27.78076	75	−15.3	bar/inclined disk
COMAi125845.906p274655.90	194.69126	27.78219	75	−14.7	bar/inclined disk

Notes. (1) Galaxy ID as given in the Coma Treasury survey DR2 (Hammer et al. 2010); (2) R.A. (J2000); (3) Decl. (J2000); (4) *HST* visit number; (5) $M_{I(814)}$ absolute magnitude in AB mag; (6) type of disk structure detected through unsharp masking (see Section 4.2).

2009). Lisker et al. (2006) search through 476 Virgo early-type dwarfs and find unambiguous stellar disk structure (bar/spiral) in 14 of them, while another 27 have probable or possible disk features. Some authors have speculated that anywhere from 5% to 50% of Virgo early-type dwarfs have disk structure, depending on the magnitude range under scrutiny (Lisker et al. 2006; Lisker & Fuchs 2009).

Approaching the search for disks in early-type dwarfs a different way, Aguerri et al. (2005) investigate a sample of galaxies in Coma with $-18 \leqslant M_B \leqslant -16$ and classify them

into two types dE or dS0 depending on their surface brightness profile. Galaxies whose surface brightness profiles are well fitted by a single Sérsic law are classified as dEs, and those with surface brightness profiles fitted with a Sérsic plus exponential profile are classified as dS0s. Aguerri et al. (2005) find that about 30% of their Coma dwarf sample cannot be fitted well by a single Sérsic law, suggesting that early-type dwarfs with disks may not be scarce in Coma. Graham & Guzmán (2003) found evidence for outer disks in three out of a sample of 18 Coma early-type dwarfs, modeling the surface brightness profiles using a Sérsic function in combination with either a central point source or a resolved central Gaussian component using high-resolution *HST* images.

While it is still unclear whether all early-type dwarfs with disk structure represent a distinct class of galaxies that are the product of a single formation mechanism, one plausible scenario is that they are formed through processing of faint, late-type spirals and irregulars in cluster environments (e.g., Kormendy 1985; Lin & Faber 1983; Graham et al. 2003; Lisker et al. 2006). This processing includes the loss of their gas through ram-pressure stripping (e.g., Gunn & Gott 1972) as well as the cumulative effects of harassment in a cluster environment (e.g., Moore et al. 1996). The simulations of Mastropietro et al. (2005) have shown that indeed late-type spirals can be reprocessed into early-type dwarfs through cluster processes (such as harassment) and that these dwarfs do retain their stellar disk structure. On the other hand, observations of a small number of isolated early-type dwarf galaxies (e.g., Fuse 2008; Hernández-Toledo et al. 2010) argue against cluster transformation processes as the sole explanation for the formation of these objects.

We find evidence of only 13 dwarfs hosting disk instabilities (bar and/or spiral arms) in our unsharp-masked subsample of 333 dwarfs. This result is in broad agreement with the findings of Méndez-Abreu et al. (2010), who find a paucity of barred disks for Coma galaxies fainter than $M_r = -17$. As also suggested by Méndez-Abreu et al. (2010), these results imply that although it is possible that as many as ∼30% of dwarf galaxies in Coma may have a disk component (Aguerri et al. 2005), the majority do not have the necessary conditions to form or maintain bar and spiral instabilities, namely, a disk that is dynamically cold. This result is consistent with previous studies, showing a paucity of *thin* disks in lower-luminosity dwarf galaxies (Sánchez-Janssen et al. 2010; Yoachim & Dalcanton 2006).

5. SUMMARY

We use ACS F814W images from the *HST* ACS Treasury survey of the Coma cluster at $z \sim 0.02$ to study the fraction and properties of barred galaxies in the central region of Coma, the densest environment in the nearby universe. The available data span 274 arcmin^2, where approximately 75% of the data are within 0.5 Mpc of the cluster center, and contain thousands of sources down to a limiting magnitude of $I = 26.8$ mag in F814W (AB mag). We initially select 469 cluster members and split the sample with a magnitude cut at $M_V \lesssim -18$ (Vega mag). Using this magnitude cut, we investigate two different regimes: (1) the fraction and properties of bright $M_V \lesssim -18$ S0 galaxies and (2) the presence of bars and other disk features (e.g., bars and spiral arms) in faint/dwarf galaxies in the Coma core. Our results for the two populations are described below.

1. For S0 galaxies: we select a sample of 32 bright S0 galaxies based on visual classification supplemented by multi-component decompositions in ambiguous cases (Section 3.1). After discarding 12 highly inclined galaxies, we identify and characterize bars in the remaining 20 moderately inclined S0s using three methods: ellipse fits where the bar is detected through strict criteria (the peak bar ellipticity e_{bar} is required to be a global maximum in the radial profile of ellipticity), ellipse fits where the bar is detected through relaxed criteria (which do not require the peak bar ellipticity e_{bar} to be a global maximum), and visual classification. We find:
   (a) the optical bar fraction for our bright S0 sample is: 50% ± 11%, 65% ± 11%, and 60% ± 11% based on ellipse fits with traditional and relaxed criteria, and visual classification, respectively (Table 2).
   (b) We compare to results from studies in less dense environments (A901/902 and Virgo) and find that the bar fraction, as well as the mean quantitative properties of the S0 bars and disks (e.g., R_{25}, a_{bar}, e_{bar}), do not show a statistically significant variation, within the error bars, for samples of matched S0s in environment densities ranging from $n \sim 300$ galaxies Mpc^{-3} (Virgo), $n \sim 1000$ galaxies Mpc^{-3} (A901/902), and $n \sim$10,000 galaxies Mpc^{-3} (Coma), with high galaxy velocity dispersions $\sigma \sim 800$ km s^{-1} (Table 3, Figure 14). We note that there is a hint that the mean bar fraction may show a slight increase as a function of environment density toward the dense core of the Coma cluster (Figure 11), however given the error bars, we cannot say whether this trend is significant. We speculate that the bar fraction among S0s is not dramatically enhanced in rich clusters compared to low-density environments due to several factors. First S0s in rich clusters are likely to be more stable to bar instabilities because they are dynamically heated by the cumulative effect of many high-speed, weak encounters (galaxy harassment) and additionally are gas poor as a result of ram pressure stripping and accelerated star formation. Second, individual high-speed encounters in rich clusters may be less effective than individual slow strong encounters in inducing bars. The combination of these effects precludes an enhancement in the bar fraction for S0 galaxies in cluster environments compared to the field. Our results are in agreement with recent observational studies which find no difference in the fraction of barred galaxies with environment density over all Hubble types.
2. For faint/dwarf galaxies: we select a sample of 417 galaxies fainter than $M_{I(814)} = -18.5$ (AB mag; Section 4.1) where we utilize our ∼50 pc resolution to look for disk structures such as bars and spiral arms using visual classification of unsharp-masked images. After applying unsharp masking to a subsample of 333 dwarfs ($\mu_e < 25$ mag arcsec^{-2}, $R_{90} > 100$ pc; Section 4.2), we find only 13 dwarf galaxies with a bar and/or spiral arms, and an additional eight galaxies where an inclined disk may be present (Figure 17). These results suggest that either disks are not common in these galaxies in the Coma cluster core or that any disks present are too hot to form instabilities.

I.M., S. J., and T. W. acknowledge support from the National Aeronautics and Space Administration (NASA) LTSA grant NAG5-13063, NSF grant AST-0607748, and *HST* grants GO-11082 and GO-10861 from STScI, which is operated by AURA, Inc., for NASA, under NAS5-26555. S.J. thanks the Excellence

Cluster Origin and Structure of the Universe in Garching, Germany, sponsored by TUM, the Ludwig-Maximilians-Universitt (LMU), the Max-Planck-Institutes, and the European Southern Observatory (ESO). P.E. was supported by DFG Priority Program 1177 ("Witnesses of Cosmic History: Formation and evolution of black holes, galaxies and their environment"). D.C. acknowledges support from the UK Science and Technology Facilities Council under grant ST/H002391/1.

REFERENCES

Abraham, R. G., Merrifield, M. R., Ellis, R. S., Tanvir, N. R., & Brinchmann, J. 1999, MNRAS, 308, 569
Aguerri, J. A. L., & González-García, A. C. 2009, A&A, 494, 891
Aguerri, J. A. L., Iglesias-Páramo, J., Vílchez, J. M., Muñoz-Tuñón, C., & Sánchez-Janssen, R. 2005, AJ, 130, 475
Aguerri, J. A. L., Méndez-Abreu, J., & Corsini, E. M. 2009, A&A, 495, 491
Andersen, V. 1996, AJ, 111, 1805
Athanassoula, E. 2005, MNRAS, 358, 1477
Balogh, M. L., Baldry, I. K., Nichol, R., et al. 2004, ApJ, 615, L101
Barazza, F. D., Binggeli, B., & Jerjen, H. 2002, A&A, 391, 823
Barazza, F. D., Jablonka, P., Desai, V., et al. 2009, A&A, 497, 713
Barazza, F. D., Jogee, S., & Marinova, I. 2008, ApJ, 675, 1194 (BJM08)
Barazza, F. D., Jogee, S., Rix, H.-W., et al. 2006, ApJ, 643, 162
Bell, E. F., McIntosh, D. H., Katz, N., & Weinberg, M. D. 2003, ApJS, 149, 289
Bell, E. F., Papovich, C., Wolf, C., et al. 2005, ApJ, 625, 23
Bell, E. F., Phleps, S., Somerville, R. S., et al. 2006, ApJ, 652, 270
Binggeli, B., & Cameron, L. M. 1991, A&A, 252, 27
Binggeli, B., Sandage, A., & Tammann, G. A. 1988, ARA&A, 26, 509
Binggeli, B., Tammann, G. A., & Sandage, A. 1987, AJ, 94, 251
Binney, J., & Tremaine, S. 1987, Galactic Dynamics (Princeton, NJ: Princeton Univ. Press)
Blanton, M. R., Eisenstein, D., Hogg, D. W., Schlegel, D. J., & Brinkmann, J. 2005, ApJ, 629, 143
Block, D. L., Buta, R., Knapen, J. H., et al. 2004, AJ, 128, 183
Borch, A., Meisenheimer, K., Bell, E. F., et al. 2006, A&A, 453, 869
Buta, R., & Crocker, D. A. 1993, AJ, 106, 939
Byrd, G., & Valtonen, M. 1990, ApJ, 350, 89
Cameron, E., Carollo, C. M., Oesch, P., et al. 2010, MNRAS, 409, 346
Carter, D. 1978, MNRAS, 182, 797
Carter, D. 1987, ApJ, 312, 514
Carter, D., Goudfrooij, P., Mobasher, B., et al. 2008, ApJS, 176, 424
Chilingarian, I. V., Cayatte, V., Durret, F., et al. 2008, A&A, 486, 85
Colbert, J. W., Mulchaey, J. S., & Zabludoff, A. I. 2001, AJ, 121, 808
Combes, F., Debbasch, F., Friedli, D., & Pfenniger, D. 1990, A&A, 233, 82
Combes, F., & Sanders, R. H. 1981, A&A, 96, 164
de Vaucouleurs, G., de Vaucouleurs, A., Corwin, H. G., Jr., et al. 1991, Third Reference Catalogue of Bright Galaxies (New York: Springer) (RC3)
Dressler, A. 1980, ApJ, 236, 351
Dubinski, J. 1994, ApJ, 431, 617
Elmegreen, D. M., Elmegreen, B. G., & Bellin, A. D. 1990, ApJ, 364, 415
Elmegreen, B. G., Elmegreen, D. M., & Hirst, A. C. 2004, ApJ, 612, 191
Erwin, P. 2005, MNRAS, 364, 283
Erwin, P., & Sparke, L. S. 2003, ApJS, 146, 299
Eskridge, P. B., Frogel, J. A., Pogge, R. W., et al. 2000, AJ, 119, 536
Friedli, D., Wozniak, H., Rieke, M., Martinet, L., & Bratschi, P. 1996, A&AS, 118, 461
Fuse, C. R. 2008, PhD thesis, Texas Christian Univ.
Gadotti, D. A. 2008, MNRAS, 384, 420
Gadotti, D. A. 2011, MNRAS, 415, 3308
Gerin, M., Combes, F., & Athanassoula, E. 1990, A&A, 230, 37
Giordano, L., Tran, K.-V. H., Moore, B., & Saintonge, A. 2010, arXiv:1002.3167 (G10)
Giuricin, G., Mardirossian, F., Mezzetti, M., & Monaco, P. 1993, ApJ, 407, 22
Gnedin, O. Y. 2003, ApJ, 589, 752
Graham, A. W., & Guzmán, R. 2003, AJ, 125, 2936
Graham, A. W., Jerjen, H., & Guzmán, R. 2003, AJ, 126, 1787
Gray, M. E., Wolf, C., Barden, M., et al. 2009, MNRAS, 393, 1275
Gunn, J. E., & Gott, J. R., III 1972, ApJ, 176, 1
Hammer, D., Verdoes, K. G., Hoyos, C., et al. 2010, ApJS, 191, 143
Heiderman, A., Jogee, S., Marinova, I., et al. 2009, ApJ, 705, 1433
Heller, C. H., & Shlosman, I. 1994, ApJ, 424, 84
Heller, C. H., Shlosman, I., & Athanassoula, E. 2007, ApJ, 671, 226
Hernández-Toledo, H. M., Vázquez-Mata, J. A., Martínez-Vázquez, L. A., Choi, Y.-Y., & Park, C. 2010, AJ, 139, 2525
Hernquist, L. 1989, Nature, 340, 687
Hogg, D. W. SDSS Collaboration 2003, BAAS, 35, 770
Hohl, F. 1975, in IAU Symp. 69, Dynamics of the Solar Systems, ed. A. Hayli (Dordrecht: Reidel), 349
Hoyos, C., den Brok, M., Kleijn, G. V., et al. 2011, MNRAS, 411, 2439
Hunt, L. K., & Malkan, M. A. 1999, ApJ, 516, 660
Jedrzejewski, R. I. 1987, MNRAS, 226, 747
Jerjen, H., Kalnajs, A., & Binggeli, B. 2000, A&A, 358, 845
Jester, S., Schneider, D. P., Richards, G. T., et al. 2005, AJ, 130, 873
Jogee, S. 1999, PhD thesis, Yale Univ.
Jogee, S. 2006, in Physics of Active Galactic Nuclei at all Scales, ed. D. Alloin, R. Johnson, & P. Lira (Lecture Notes in Physics, Vol. 693; Berlin: Springer), 143
Jogee, S., Barazza, F., Rix, H.-W., et al. 2004, ApJ, 615, L105
Jogee, S., Knapen, J. H., Laine, S., et al. 2002a, ApJ, 570, L55
Jogee, S., Miller, S. H., Penner, K., et al. 2009, ApJ, 697, 1971
Jogee, S., Scoville, N., & Kenney, J. D. P. 2005, ApJ, 630, 837
Jogee, S., Shlosman, I., Laine, S., et al. 2002b, ApJ, 575, 156
Kazantzidis, S., Kravtsov, A. V., Zentner, A. R., et al. 2004, ApJ, 611, L73
Knapen, J. H., Shlosman, I., & Peletier, R. F. 2000, ApJ, 529, 93
Kormendy, J. 1979, ApJ, 227, 714
Kormendy, J. 1985, ApJ, 295, 73
Kormendy, J. 1993, in IAU Symp. 153, Galactic Bulges, ed. H. DeJonghe & H. J. Habing (Dordrecht: Kluwer), 209
Kormendy, J., & Fisher, D. B. 2008, in ASP Conf. Ser. 396, Formation and Evolution of Galaxy Disks, ed. J. G. Funes & E. M. Corsini (San Francisco, CA: ASP), 297
Kroupa, P., Tout, C. A., & Gilmore, G. 1993, MNRAS, 262, 545
Laine, S., Shlosman, I., Knapen, J. H., & Peletier, R. F. 2002, ApJ, 567, 97
Larson, R. B., Tinsley, B. M., & Caldwell, C. N. 1980, ApJ, 237, 692
Laurikainen, E., Salo, H., & Buta, R. 2005, MNRAS, 362, 1319
Laurikainen, E., Salo, H., Buta, R., & Knapen, J. H. 2007, MNRAS, 381, 401
Laurikainen, E., Salo, H., Buta, R., & Knapen, J. H. 2009, ApJ, 692, L34
Laurikainen, E., Salo, H., Buta, R., & Vasylyev, S. 2004, MNRAS, 355, 1251
Lin, D. N. C., & Faber, S. M. 1983, ApJ, 266, L21
Lisker, T., & Fuchs, B. 2009, A&A, 501, 429
Lisker, T., Grebel, E. K., & Binggeli, B. 2006, AJ, 132, 497
Lisker, T., Grebel, E. K., Binggeli, B., & Glatt, K. 2007, ApJ, 660, 1186
Marinova, I., & Jogee, S. 2007, ApJ, 659, 1176 (MJ07)
Marinova, I., Jogee, S., Heiderman, A., et al. 2009, ApJ, 698, 1639 (M09)
Mastropietro, C., Moore, B., Mayer, L., et al. 2005, MNRAS, 364, 607
Matković, A., & Guzmán, R. 2005, MNRAS, 362, 289
Mendez, M., Orsatti, A. M., & Forte, J. C. 1989, ApJ, 338, 136
Méndez-Abreu, J., Sánchez-Janssen, R., & Aguerri, J. A. L. 2010, ApJ, 711, L61
Menéndez-Delmestre, K., Sheth, K., Schinnerer, E., Jarrett, T. H., & Scoville, N. Z. 2007, ApJ, 657, 790
Mihos, J. C., & Hernquist, L. 1996, ApJ, 464, 641
Mobasher, B., Colless, M., Carter, D., et al. 2003, ApJ, 587, 605
Moore, B., Katz, N., Lake, G., Dressler, A., & Oemler, A. 1996, Nature, 379, 613
Mulchaey, J. S., & Regan, M. W. 1997, ApJ, 482, L135
Nair, P. B., & Abraham, R. G. 2010a, ApJ, 714, L260
Nair, P. B., & Abraham, R. G. 2010b, ApJS, 186, 427
Noguchi, M. 1988, A&A, 203, 259
Odewahn, S. C. 1996, in ASP Conf. Ser. 91, IAU Colloq. 157, Barred Galaxies, ed. R. Buta, D. A. Crocker, & B. G. Elmegreen (San Francisco, CA: ASP), 30
Peng, C. Y., Ho, L. C., Impey, C. D., & Rix, H.-W. 2002, AJ, 124, 266
Quilis, V., Moore, B., & Bower, R. 2000, Science, 288, 1617
Reese, A. S., Williams, T. B., Sellwood, J. A., Barnes, E. I., & Powell, B. A. 2007, AJ, 133, 2846
Regan, M. W., & Elmegreen, D. M. 1997, AJ, 114, 965
Regan, M. W., Vogel, S. N., & Teuben, P. J. 1997, ApJ, 482, L143
Robaina, A. R., Bell, E. F., Skelton, R. E., et al. 2009, ApJ, 704, 324
Romano-Díaz, E., Shlosman, I., Heller, C., & Hoffman, Y. 2008, ApJ, 687, L13
Sakamoto, K., Okumura, S. K., Ishizuki, S., & Scoville, N. Z. 1999, ApJ, 525, 691
Sánchez-Janssen, R., Méndez-Abreu, J., & Aguerri, J. A. L. 2010, MNRAS, 406, L65
Sandage, A., & Binggeli, B. 1984, AJ, 89, 919
Schneider, P. (ed.) 2006, Extragalactic Astronomy and Cosmology (Berlin: Springer)
Schwarz, M. P. 1981, ApJ, 247, 77
Schweizer, F., & Ford, W. K., Jr. 1985, in New Aspects of Galaxy Photometry, ed. J. L. Nieto (Lecture Notes in Physics, Vol. 232; Berlin: Springer), 145
Sheth, K., Elmegreen, D. M., Elmegreen, B. G., et al. 2008, ApJ, 675, 1141

Sheth, K., Regan, M. W., Scoville, N. Z., & Strubbe, L. E. 2003, ApJ, 592, L13
Sheth, K., Vogel, S. N., Regan, M. W., Thornley, M. D., & Teuben, P. J. 2005, ApJ, 632, 217
Steinmetz, M., & Navarro, J. F. 2002, New Astron., 7, 155
Tago, E., Einasto, J., Saar, E., et al. 2008, A&A, 479, 927
The, L. S., & White, S. D. M. 1986, AJ, 92, 1248
Thompson, L. A. 1981, ApJ, 244, L43 (T81)
Trentham, N. 1998, MNRAS, 293, 71
Trentham, N., & Hodgkin, S. 2002, MNRAS, 333, 423
Toomre, A. 1981, Structure and Evolution of Normal Galaxies (Cambridge: Cambridge Univ. Press), 111
van den Bergh, S. 2002, AJ, 124, 782
van Zee, L. 2001, AJ, 121, 2003
Varela, J., Moles, M., Márquez, I., et al. 2004, A&A, 420, 873
Weinzirl, T., Jogee, S., Khochfar, S., Burkert, A., & Kormendy, J. 2009, ApJ, 696, 411
Wolf, C., Aragón-Salamanca, A., Balogh, M., et al. 2009, MNRAS, 393, 1302
Wolf, C., Bell, E. F., McIntosh, D. H., et al. 2005, ApJ, 630, 771
Wozniak, H., Friedli, D., Martinet, L., Martin, P., & Bratschi, P. 1995, A&AS, 111, 115
Yoachim, P., & Dalcanton, J. J. 2006, AJ, 131, 226